

INVESTIGATION OF THE PROCESSES OF RETENTION AND RELEASE OF IMPLANTED DEUTERIUM AND HELIUM IONS FOR TUNGSTEN AND TANTALUM COATINGS

 M.O. Azarenkov^b,  V.V. Bobkov^{a,*},  L.P. Tishchenko^a, Yu.I. Kovtunenکو^a,  A.O. Skrypnyk^a,
 D.I. Shevchenko^a,  L.O. Gamayunova^a

^a V. N. Karazin Kharkiv National University, 4, Svobody Sq., Kharkiv, 61022, Ukraine

^b National Science Center "Kharkov Institute of Physics and Technology", 1, Akademichna St., Kharkiv, 61108, Ukraine

*Corresponding Author e-mail: bobkov@karazin.ua

Received November 1, 2023; revised December 6, 2023; accepted December 15, 2023

The analysis of main published results of studies of retention and migration of ion-implanted hydrogen isotopes and helium in tungsten and tantalum coatings, formation of radiation damages of the crystal lattice and their interaction with implanted gases, as well as the influence of helium and deuterium on various properties and surface morphology of coatings was carried out. The irradiation of samples was performed by beams of accelerated ions of hydrogen isotopes or He⁺, and in a plasma containing these ions, at various fluences and energies of incident ions, and at various temperatures of targets during implantation. Special attention was paid to the research results obtained at simultaneous irradiation of W both in bulk and in thin-film form. The used methods were electron microscopy, reemission mass spectrometry, thermal desorption spectrometry, X-ray photoelectron spectroscopy, X-ray diffraction, nuclear reaction analysis and Rutherford ion scattering.

Keywords: Deuterium; Helium; Ion implantation; Thermal desorption; Retention; Damage; W and Ta coatings

PACS: 61.80.-x, 61.80.Jh

INTRODUCTION

At present, most of the world's electricity demands are satisfied by fossil fuels, mainly oil, natural gas and coal. According to the conclusions of the Intergovernmental Panel on Climate Change, a noticeable increase in temperature in the last century is a result of a significant increase in greenhouse gas emissions, including CO₂, due to the use of these sources. To prevent dangerous climate change, the current energy supply system must change significantly. We need new sources of energy with renewable resources. These are the energies of the sun, wind, biomass, hydropower, which are fully mastered or in the process of development. However, they are not always available, are unstable, subject to sudden climate change, and require additional equipment for concomitant energy storage. Precisely for this reason energy sources based on nuclear fission have been adopted by many developed countries. Existing nuclear power plants are long-term sources of energy, and the used fuel has little impact on the environment. However, natural cataclysms led to the destruction of station blocks and the release of radioactive products of nuclear reactions.

Recent researches of controlled fusion have shown that this new energy source can produce environmentally safe electricity, has rich fuel resources that will satisfy the needs of the growing population of a world. In a fusion reaction, the released amount of energy is about four million times higher than the amount of energy released when burning coal. However, as Pranevičius et al. noted [1], the successful operation of fusion power plants requires the use of plasma-facing materials (PFM) with certain parameters. First, they must withstand high temperatures. The surface temperature can reach 1073 K, but in some areas and during transients, this temperature can exceed 2273 K. The material must work under intense X-rays and gamma radiation, be resistant to bombardment by produced in the fusion reaction high-intensity accelerated neutrons with energy of ~ 14 MeV, and to the impact during plasma disruption of intense flows of hydrogen isotopes and helium with a density of 10²² m⁻²·s⁻¹ – 10²⁴ m⁻²·s⁻¹ and the energies from several eV to tens of keV. The mechanical and physical properties of PFM are changed including erosion and subsequent impurities transfer, which leads to mixing of the materials of these devices. At this, the plasma becomes contaminated with eroded particles of impurities. Getting into the plasma, they cause its radiation losses, which are proportional to the atomic number Z of the impurity. This additionally leads to the plasma cooling and disruption of the fusion reaction. High-energy neutrons and tritium, interacting with the walls of the plasma chamber and internal vessels, activate materials. Retention of great amounts of tritium in the PFM increases the cost of fuel in the reactor and presents a safety problem. It is possible to reduce the level of radioactivity and resist the deterioration of mechanical and physical properties, as well as erosion, by developing radiation-resistant structural materials. The main requirements for PFM are as follows: good mechanical and physical properties, excellent resistance to high temperature cyclic loads, low sputtering ratio, insensitivity to chemical sputtering, low tritium retention, low activation by neutron irradiation, and low Z.

The processes in a solid as a result of irradiation with accelerated ions of hydrogen isotopes (H⁺, D⁺, T⁺) and He⁺ or as a result of exposure to containing the listed ions plasma, can be both inelastic and elastic. At the inelastic interaction, electron radiation, X-ray and light radiation, and heating of a solid are observed. Their influence on the properties of the

irradiated layers is negligible. The elastic interaction of ions with a solid causes desorption of atoms adsorbed on the surface, emission of neutrals, excited atoms and ions, formation of crystal lattice defects, and retention of bombarding ions in the bulk. The energy of elastic interaction of H^+ , D^+ , T^+ , and He^+ ions with tungsten, for example, should exceed ~ 2050 eV, ~ 960 eV, ~ 700 eV, and ~ 480 eV respectively, as it is shown in [2] and [3]. The adsorption and desorption processes are determined mainly by the properties of the upper monolayer of the solid. Ion-photon emission and secondary ion emission are very sensitive to the composition, structure and morphology of the target surface. The emission of sputtered atoms occurs from depths of 2–3 monolayers and in many cases can be considered as a surface process. The formation of radiation defects in the crystal lattice and the retention of bombarding ions in the volume (implantation) depend on the energy of the ions. Schematic representation of the dominant processes during irradiation with ions of different energies is shown in Figure 1 [1].

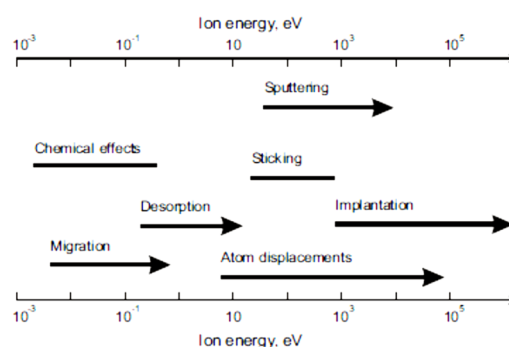


Figure 1. Schematic presentation of the dominant processes under irradiation by ions of different energies [1].

The dominant processes are determined by the type of ions, their energy, mass, charge state, intensity of ion irradiation, and properties of the target material. In plasma, due to very high ion flux densities, even at low energy, radiation damages of the target can occur in the result of the local supersaturating with particles.

For ITER, according to estimation of Yoshida [4], hydrogen ions, that bombarded divertor plates, have a flux and average energy not high than $10^{24} \text{ m}^{-2} \text{ s}^{-1}$ and 100 eV, respectively. Therefore, one of the main problem for the divertor material is erosion due to sputtering with these high-density ions. The situation for the first wall is significantly different then for the divertor plate. The flux and the energy of hydrogen particles bombarding the first wall of ITER estimate as do not exceed $10^{20} \text{ m}^{-2} \cdot \text{s}^{-1}$ and 100–500 eV, respectively. These particles are hydrogen ions and neutrals produced in the edge plasma. In addition to these low energy particles, high energy neutrals coming out from the high temperature core will also hit the first wall. Their flux and energy as predicted are respectively $\sim 10^{18} \text{ m}^{-2} \cdot \text{s}^{-1}$ and 10 keV. Although the number of neutrals on the first wall is much smaller than the number of ions on the divertor plates, they can result in significant erosion due to sputtering, as well as striking damage of materials. One of the main problems for PFM is penetration and retention of implanted hydrogen isotopes. Retention helium ion with the energy of several tens keV in the PFM [5] is also dangerous because of their intense interaction with lattice defects. Helium greatly accelerates the formation of bubbles, blisters and fuzz. As a result, local swelling and deterioration of the mechanical properties of materials occur.

Tungsten was chosen as a radiation-resistant structural material in the protective coatings of ITER devices because of its good resistance to erosion by ions and recharged particles in comparison with other materials and because of its heat resistance [6]. Tungsten has high energy threshold for physical sputtering, low tritium retention, and does not form hydrides or compounds with deposited tritium [7]. In addition, it has the highest melting point of all metals, low vapor pressure, high recrystallization temperature (1720 K), good thermal conductivity and retains strength at high temperature. This combination of physical and mechanical properties makes it suitable for use as a coating for high heat flux components. However, Jiang at al. in [8] pointed out that the disadvantages of tungsten, such as brittleness at low temperatures (the transition temperature from plastic to brittle state is ranging from 370 K to 670 K) and high weight, make difficult its processing and welding. The operating temperature of the plasma-facing (PFC) tungsten components must be above the temperature of transition.

Brossa at al. considered Ta as a radiation-resistant structural material in the protective coatings of ITER components [9]. Tantalum has a very low sputtering coefficient, low tritium retention, high melting point, low vapor pressure and good mechanical properties at low and high temperatures. Like other refractory metals, Ta does not form an arc. Significant resistance to thermal fatigue, high recrystallization temperature (1620 K), low brittle-ductile transition temperature and resistance to thermal shock permit to use tantalum in such structural components as the first wall and blanket in a tokamak, despite the high Z.

Manufacturing of products of complex shape from pure and massive tungsten or tantalum is a technologically complex and, as a result, expensive task. The promising solution for their use as PFM is to coat a functional or heat-removing PFC with a layer of these materials. Recent studies [5, 10] have shown that the most promising candidates for PFM will be nanocrystalline coatings for PFC. For such PFMs, it is possible to adapt their radiation resistance by creating a high density of grain boundaries, which are considered to be defect absorbers.

For practical use of W and Ta coatings in ITER devices, at present the study of the processes of retention and release of ion-implanted hydrogen isotopes and helium in them is very important. Analysis of the formation of matrix radiation defects, their interaction with deuterium and helium, and the influence on their behavior permits to study many fundamental parameters and regularities and determine the radiation resistance of coatings to the influence of flows of hydrogen isotope and helium ions under real ITER conditions. The development of methods for obtaining W or Ta coatings of various thicknesses with high adhesion rates, good structure and properties is also an important task.

EXPERIMENTAL PROCEDURE

In practice promising PFM for ITER tungsten or tantalum can be used as coatings deposited on PFCs. The following technologies of metal coating deposition could be used: vacuum plasma spray (VPS), plasma deposition in inert gas (IPS), chemical vapor deposition (CVD), physical vapor deposition or materials vapor deposition (PVD), magnetron sputtering of material (MS), combination of magnetron sputtering of material with ion implantation (CMSII). PFCs most often are structures from carbon based materials - CFC (carbon-fiber composite), copper, stainless steel, etc. At that, the thermal conductivity of W and Ta coatings on the PFC should be high [11]. Boir-Lavigne et al. showed relation of the thermal conductivity of W coating on its microstructure [12]. Tungsten coatings deposited on graphite by the VPS, CPS and PVD methods were investigated and tested at high thermal loads [13, 14]. Smid et al. compared tungsten coatings deposited by PVD, CVD, and VPS methods on a copper substrate [15]. According to [12, 15], the VPS method was recommended for objects in areas with a lower heat flux (below 5 MW/m²), its advantages were high metal deposition rates and a high recovery probability. CVD coatings demonstrated heat flux resistance up to 20 MW/m² [15]. However, high thermal conductivity of coatings deposited by CVD as well as PVD methods did not necessarily mean good thermal shock resistance. In addition, the disadvantages of both the latter methods were low deposition rates and high costs. In tests with a very high heat flux, W coatings with thicknesses of 0.5 μm, 1–3 μm, and 10 μm deposited by the CMSII on a CFC substrate displayed the best result [16, 17]. In [7, 18], W coatings deposited on a CFC substrate by the same method withstood tests up to 23 MW/m² (1.5 s) and a cyclic load with 200 pulses of 10.5 MW/m² (5 s) without delaminating. The surface temperature during the tests was above 2273 K. The following factors determined the obtained results: nanostructure of W coatings and a Mo interlayer, which was introduced between the coating and the substrate, removed the stresses induced in the coatings by high-energy ion bombardment. Detailed characteristics of W coatings deposited on a CFC substrate by the CMSII method were given in [7, 19, 20]. TEM (transmission electron microscopy) studies [19, 20] showed the formation of extremely dense nanostructure with crystallites less than 10 nm in size and without any pores. Ruset et al. in [7] showed that the introduction of Mo interlayer with a thickness from 2 μm to 3 μm reduced the arising at the interface stress by ~ 40%. Removing the stress at the Mo/W interface and inside the W coating permitted to fabricate coatings with a thickness of 10–30 μm. The successful use of molybdenum as an intermediate layer was also noted in [19]. This seemed to be due to the correction of the thermal expansion mismatch between CFC and W. Re also was successfully used as an intermediate layer [21, 22]. It did not form carbides, had a high melting temperature and could act as a diffusion barrier between carbon and tungsten.

In [23–26] the results of studies with optical microscopy, SEM (scanning electron microscopy), TEM, X-ray diffraction, etc. of adhesion, structure, and resistance to high thermal loads of W coatings, deposited by various methods on CFC, stainless steel, and copper substrates, were presented. Pranevičius in [23] described the preparation of W coatings on stainless steel and graphite substrates changing the deposition parameters in the MS method for obtaining coatings with improved properties. W films less than 2 μm thick on stainless steel and graphite substrates showed good adhesion in a wide range of deposition parameters: working gas pressure Ar from 0.4 Pa to 2 Pa, negative bias from 50 V to 150 V, substrate temperature from 320 K to 470 K and a distance to the substrate of 0.05–0.07 m. Adhesion to the same substrates of W films with the thickness of more than 5 μm worsened. SEM studies showed a columnar microstructure of the W films. The electrical resistance ρ of the films measured with a four-point probe scheme was 0.058 μΩ · m, and less than ρ of the bulk W. Mechanical properties, such as Vicker micro hardness, erosion resistance, and wear of the W films depended on their deposition parameters. W films obtained under intense low-energy ion irradiation with a high flux density demonstrated an improvement in mechanical properties.

Tungsten coatings VPS deposited on a copper substrate were studied by Niu et al. [24]. For improving the adhesion between the coating and the substrate, an additional intermediate layer of tungsten - copper composite was deposited. The microstructure and composition of W coatings were analyzed using SEM, TEM, XRD, and EDX methods. The structures of the coatings were mainly lamellar and contained columnar crystalline grains. Pores of irregular and linear shape were observed, they were formed as a result of unmelted or semi-molten splashes of W and the gases trapping. The porosity reached ~ 4%. Distinguished interfaces were found, consisting of tungsten oxide or micro pores between layers. The imperfect microstructure of the tungsten coatings resulted in their low thermal and electrical conductivity.

Nanostructured W coatings of thicknesses from 9 μm to 12 μm were CMSII method deposited on CFC substrates [25, 26]. The grain size was less than 10 nm with the preferred orientation of {200} planes parallel to the surface and {110} planes perpendicular to the surface. W coatings of 10 μm thick showed excellent thermal resistance at high heat fluxes compared to similar coatings deposited by traditional PVD or CVD methods.

Alimov and Scherzer also reported about pores in W coatings [27], several types of coatings were studied:

– CVD-W coating 15 μm thick on a copper substrate, which had a textured structure with a grain size of 2–3 μm, a porosity not exceeding 0.04%, and a surface roughness of about 1 μm;

– IPS-W coating 200 μm thick on a graphite substrate, having a lamellar structure, porosity 15–20% and surface roughness $\sim 18 \mu\text{m}$;

– VPS-W coating 500 μm thick on a graphite substrate with an intermediate layer of rhenium from 10 μm to 20 μm thick. The last coating after the deposition process was heated for 1 h at a temperature of 1700 K; that resulted in the structure recrystallization with a porosity of $\sim 8\text{--}9\%$ and a surface roughness of about 4 μm .

Bizyukov et al. [28] in MS-W films on substrates of polished pyrolytic graphite studied their mechanical and thermal properties, surface erosion, and retention of hydrogen isotopes. For reducing mechanical stresses occurred on the coating-substrate interface, an intermediate layer of copper was deposited.

The result of studies of Ta coatings deposited by CVD and VPS methods on Al, Cu, AISI 316L, and Inconel 600 substrates were represented in [9]. The mechanical properties of Ta coatings and the conditions that improve their adhesion to the substrates were studied. The authors showed that tantalum coatings could be used to reduce the erosion of components subjected to short-term but intense thermal loads. CVD and VPS were good methods for their deposition with good adhesion on various metals. Under powerful heat fluxes CVD-Ta coatings were destroyed only after the melting of the base material of the substrate. Powerful mechanical deformation led to the formation of cracks in the VPS-Ta coatings, but without detachment from the substrate. The presence of porosity of VPS-Ta coatings enhanced the process of hydrogen isotopes and helium release into vacuum. Taylor and Green considered the possibility of using Ta coatings of 1 mm thick, VPS deposited on ferritic steel pipes for the first wall of the ICF reactor chamber [29]. The coatings demonstrated good mechanical properties that completely remained under low-cyclic high-temperature loads concerned with the reactor work.

The dependence of mechanical properties of Ta coatings on their structure was showed in [30]. The authors studied the evolution of the structure of deposited tantalum films to select the parameters of MS deposition of high-quality single-phase Ta coatings with thicknesses from 1 μm to hundreds μm on steel. Bulk tantalum had a crystallographic bcc structure, also known as the α -phase, hard and ductile, with a Knoop hardness of 300–400 and a relatively low electrical resistivity ($0.135 \mu\Omega \cdot \text{m}$). In deposited tantalum films ([31, 32]) tetragonal structure, also known as the β phase, was identified. This metastable phase was hard (Knoop hardness greater than 900), brittle and had an electrical resistivity of an order of magnitude higher than the α -phase. The deposition of high-quality thick tantalum films was problematic because the β -phase dominated in the coatings on most substrates at different processing parameters. To stimulate the predominant growth of the α -phase, the choice of special deposition conditions, substrates or the deposition of interfacial layers were required [33, 34]. In [21, 30], the growth of the pure α -phase of tantalum was achieved by heating steel substrates during the deposition to the temperature of $\sim 670 \text{ K}$, at which the properties of steel did not deteriorate.

The authors of this work studied tungsten and tantalum coatings deposited by the MS method on stainless steel. The deposition technique was described in details in [35–37]. Coatings were prepared by sputtering W or Ta targets in Ar atmosphere at the pressure of 1.0 Pa. The coatings were deposited on a 0.8 mm thick substrate with a Ti layer of less than 10 nm thick predeposited on it at the temperature $T = 600 \text{ K}$ and at the rate of $0.6 \text{ nm} \cdot \text{s}^{-1}$. In some cases, stainless steel with Ti sublayer up to 10 nm thick was additionally coated with 3 μm thick Cu layer, then a Ti sublayer less than 10 nm thick, and then W layer. The thicknesses of the W coatings were in the range 0.1–1.0 μm or 2.2 μm . The Ta coatings were 1.5 μm thick. The W and Ta coatings had a polycrystalline bcc structure with an average grain size from 20 nm to 60 nm and were considered as nanocrystalline.

RESULTS AND DISCUSSION

Hydrogen (deuterium) implantation, retention and release from tungsten coatings

Proper design of a fusion reactor is not possible without understanding the hydrogen isotopes (protium, deuterium, and tritium) retention and recycling for plasma-facing components [38]. Recycling is the return of cold hydrogen into plasma. As a result, the plasma temperature decreases. Hydrogen isotopes trapping is especially important for tritium. The retention of great amounts of tritium in components facing the reactor plasma increases the cost of fuel in the reactor and offers a safety problem. Initial defects existing in the PFM and defects produced by thermonuclear neutrons and energetic ions of hydrogen isotopes can trapped atoms of these gases in the implantation zone. The traps eventually become saturated, and entrapped hydrogen isotope atoms disperse from the implantation zone, going either deeper into the material or toward the front surface. Atoms reaching any surface are not guaranteed to be released immediately. On a plasma-facing surface, except at extremely high temperatures, recombination of atoms into molecules should occur before their release is possible. A high recombination rate factor results in a rapid release of atoms reaching the surface, effectively reducing the concentration of hydrogen isotopes on the surface to zero. For hydrogen in bulk tungsten at 500 K, the recombination rate coefficients $10^{-29}\text{--}10^{-31} \text{ m}^4/\text{s}$ have been determined by many researchers. In the described below works [10, 14, 27, 28, 36, 37, 39–51] much attention has been paid to the processes of retention and release of hydrogen isotopes in tungsten coatings proposed as protect for components facing the plasma (the first wall, divertor, antenna mirrors).

W plate 1.5 mm thick and nanocrystalline tungsten film 10 μm thick, exposed to low-energy (78 eV) deuterium plasma with $\text{D}^+ > 85\%$ at the fluence of $3.9 \times 10^{24} \text{ m}^{-2}$, were analyzed in [10]. The polycrystalline W plate with purity 99.95% and density 99% from Advanced Technology & Materials Company, Ltd. was prepared by powder sintering. The tungsten film was deposited on the polycrystalline W plate (which was preliminarily kept heated to 750 K for the first 2 h

and then the temperature was lowered to 520 K for the next 8 h) by magnetron sputtering the W target in argon atmosphere (99.99% purity) at the pressure of 1 Pa on the device KYKY MP 650-A. The deposition rate was about 1 $\mu\text{m}/\text{h}$.

The W films had a grain size of less than 100 nm, a preferred (211) plane orientation, and a columnar structure perpendicular to the substrate. Samples from a polycrystalline W plate had the average grain size of about 5 μm . They were prepared by powder sintering. The samples were subjected to heat treatment at 1273 K for 1 h to relieve stress and degassing. They were polished to a mirror surface. Then, all samples were subjected to ultrasonic cleaning with acetone, alcohol, and boiled water for 15 min. The samples prepared in this way were used for irradiation in deuterium plasma as well as a substrate for the deposition of W films,.

For comparison the results for the W plate and the deposited W film, both types of samples were irradiated simultaneously. Changes in surface morphology and deuterium retention in both samples were determined using SEM and TDS, respectively. After exposure to deuterium plasma, several blisters with a size of several micrometers were observed on the surface of the W plate. The surface morphology of the tungsten film after exposure to deuterium plasma did not change (see Figure 2).

The trapping of deuterium in both samples was determined with a special installation, in a chamber evacuated to a pressure of less than 5×10^{-6} Pa. The sample was heated to 1373 K at the rate $\alpha = 1$ K/s. The desorbed gases components, including H_2O , O_2 , HDO, HD, and D_2 , were analyzed by a quadrupole mass spectrometer. The amounts of D_2 and HD were measured using a calibrated leak. The yield of HD relative to D_2 was below 4%. Absolute values of the HDO and D_2O signals were very low. Thermal desorption spectra of D_2 from both samples were compared. The total retention of deuterium was estimated by integrating the D_2 and HD thermal desorption spectra.

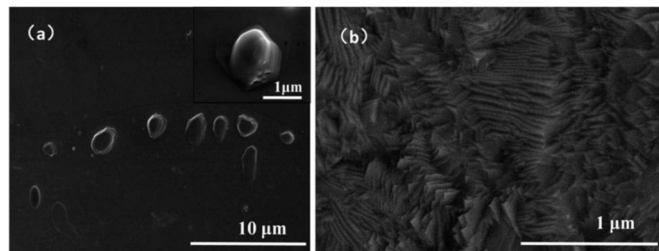


Figure 2. Surface morphologies of two different samples exposed to deuterium plasma: (a) polycrystalline tungsten plate and (b) nanocrystalline tungsten film [10].

The deuterium thermal desorption spectra for the tungsten plate and for the tungsten film differed significantly (see Figure 3). For polycrystalline tungsten the D_2 spectrum had two peaks with a maximum at the temperatures $T_{\text{max}} = 490$ K and 670 K, respectively. They could be associated with deuterium trapping by grain boundaries (GBs) and by dislocations and vacancies. Noise peaks in the vicinity of 490 K could be attributed to the explosive release of deuterium due to the rupture of gas-filled blisters during thermal desorption. The total amount of trapped D_2 was $2.4 \times 10^{20} \text{ m}^{-2}$.

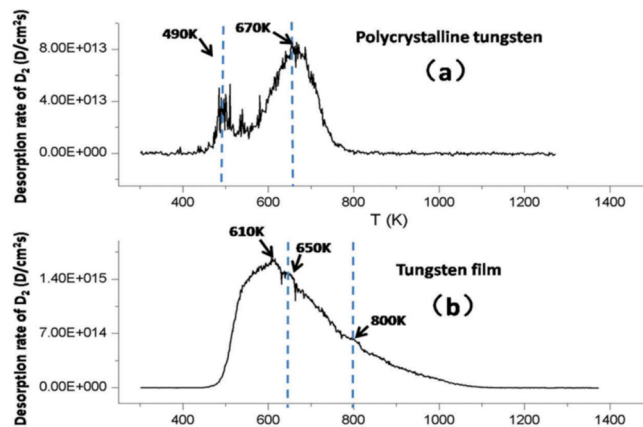


Figure 3. TDS spectra of deuterium from: (a) polycrystalline W plate, (b) nanocrystalline W film (sample heating rate $\alpha = 1$ K/s) [10].

TDS spectrum for the tungsten film had no main emission peak with a maximum at the temperature $T_{\text{max}} = 670$ K. It was characterized by a wide temperature range of D_2 release from 500 K to 1100 K and two weak peaks at temperatures of ~ 650 K and ~ 800 K. The main peak with $T_{\text{max}} = 610$ K and a peak near 650 K could be related to deuterium trapping on GBs and by dislocations and vacancies, respectively. For the higher temperature peak at 800 K deuterium trapping sites could be pores or the inner side of the vacancy cluster. The long desorption tail after 820 K, extending up to 1100 K, was attributed to the deuterium release from defects at different distances from the surface, since a large number of GBs acted as preferred diffusion channels for deuterium. The total amount of retained deuterium in the tungsten film was $6.9 \times 10^{21} \text{ m}^{-2}$, which was 30 times higher than for the W plate. So the form of the deuterium thermal desorption spectra

and the amount of trapping deuterium for the tungsten film and the tungsten plate differed significantly. The tungsten film had a nanocrystalline structure. The behavior of deuterium during irradiation was largely affected by the high density of grain boundaries. The W film showed a typical columnar structure perpendicular to the substrate, which could be the reason for the diffusion of deuterium into the material. Many intrinsic defects and a high density of grain boundaries could significantly increase the deuterium saturation threshold and deuterium retention. In addition, compressive stresses in MS-deposited tungsten film could be unfavorable for the formation of blisters and suppressed their formation to some extent.

Garcia-Rosales et al. studied trapping and thermal desorption of deuterium implanted in rolled tungsten and in two types of W coatings [14]. Both coatings were deposited on fine grain graphite substrates by the plasma spray method. The first, PVS-W coating 500 μm thick, provided by Plansee AG, was deposited in a vacuum. The second, CPS-W sample 200 μm thick was provided by CEN Cadarache (France) and was deposited in an Ar atmosphere. 10 μm thick intermediate layer of rhenium was deposited on the graphite substrate before chemical vapor deposition of the PVS-W coating to prevent the diffusion of graphite into a tungsten coating and the formation of tungsten carbide. After the coating deposition, the first sample was annealed at high-temperature (for 1 h at 1670 K). At that the coating recrystallized. No intermediate rhenium layer was in the CPS-W coating, and the sample was not high-temperature annealed. The studied samples had different porosity: rolled W at the level of 1%, PVS-W of 8–9%, CPS-W of 19–20%. Since the deposition and subsequent cooling of the deposited layer in a vacuum with an inert gas as the main component of the residual gas, no tungsten oxides were formed on the inner surfaces of the cavities.

The samples were irradiated with D_3^+ ions (300 eV) at a room temperature. Fluences were from $1 \times 10^{21} \text{ m}^{-2}$ to $1 \times 10^{22} \text{ m}^{-2}$. The flux density of D^+ ions (100 eV) was $4.4 \times 10^{19} \text{ m}^{-2} \cdot \text{s}^{-1}$. The thermal desorption spectra of deuterium for rolled W was got at a heating from room temperature to 1400 K with the rate $\alpha = (5 \pm 0.5) \text{ K/s}$ and had two peaks with $T_{\text{max}} = 475 \text{ K}$ and 850 K, while the concentration of trapped deuterium was $C = 1.6 \times 10^{20} \text{ m}^{-2}$. TDS spectra of deuterium from PVS-W also had two peaks with $T_{\text{max}} = 525 \text{ K}$ and $T_{\text{max}} = 670 \text{ K}$ and $C = 2.6 \times 10^{20} \text{ m}^{-2}$; for CPS-W in spectra there was one peak with $T_{\text{max}} = 612 \text{ K}$, and $C = 4.4 \times 10^{20} \text{ m}^{-2}$. The authors related the higher concentrations of trapped deuterium to higher porosity of the samples. Numerous gas-metal interfaces were in the volume of the porous material. The release of hydrogen from such a material could include multi-stage adsorption and desorption processes, thereby slowing down the release of deuterium from the sample. Deuterium was trapped mainly in pores and at grain boundaries.

Alimov and Scherzer studied the deuterium retention in tungsten materials with various structures at temperatures from 300 K up to 900 K using re-emission mass spectrometry (RMS), thermal desorption spectrometry (TDS), and nuclear reaction analysis (NRA). Five types of tungsten samples were investigated [27].

(i) W single crystal, 1.5 mm thick, made in State Institute of Rare Metals (Moscow) by double electron-beam zone melting. The surface was parallel to the (112) plane and was mechanically and electrochemically polished.

(ii) Hot-rolled tungsten (powder-metallurgy product, 95 at. % W, 3 at. % C, 2 at. % O, porosity $\leq 1\%$), 0.5 mm thick. The surface was also mechanically and electrochemically polished.

(iii) Chemical vapor deposited tungsten coating, CVD-W (99 at. % W, 1 at. % O), 15 μm thick, on copper substrate (from Institute of Physical Chemistry Moscow). The coating was deposited from a mixture of tungsten fluoride and hydrogen at the temperature of $\sim 900 \text{ K}$ and had a textured structure with grain size of 2–3 μm . The porosity did not exceed 0.04% and the surface roughness was about 1 μm .

(iv) Inert gas plasma sprayed tungsten coating, IPS-W (85 at. % W, 10 at. % C, 5 at. % O), 200 μm thick, on graphite substrate (from CEN Cadarache, France). The IPS coating was produced in Ar atmosphere at pressures up to atmospheric one and had a lamellar structure typical for a quick cool down of the molten droplets after spraying. Large macro-pores were present between the individual lamellae, and the porosity was 15–20%. Surface roughness was 18 μm .

(v) Vacuum plasma sprayed tungsten coating, VPS-W (99 at. % W, 1 at. % O), 500 μm thick, deposited on graphite substrate with an intermediate rhenium layer of thickness from 10 to 20 μm (from Plansee AG, Austria). As a result of the thermal treatment after the spray process (1600–1700 K for 1 h), the VPS coatings had a very homogeneous, recrystallized structure, which did not show the characteristic lamellar structure. The surface roughness of these coatings was low (about 4 μm) and the porosity was of the order 8–9%. In experiments the carbon substrate was partly removed.

Before implantation the samples were annealed at 1200 K for 10 min. The implantation was done with 4.5 keV D_3^+ ions. The flux density of 1.5 keV D-ions was $6.4 \times 10^{18} \text{ m}^{-2} \cdot \text{s}^{-1}$. Re-emission experiments were realized at temperatures of target 300, 600, and 900 K at fluences did not exceed $3.0 \times 10^{21} \text{ m}^{-2}$. TDS was carried out on samples implanted at target temperature of 300 K and at fluences equal to Φ^{sat} . The Φ^{sat} values were $0.35 \times 10^{20} \text{ m}^{-2}$ for W single crystal, $500.0 \times 10^{20} \text{ m}^{-2}$ for hot-rolled W, $0.20 \times 10^{20} \text{ m}^{-2}$ for CVD-W, $0.45 \times 10^{20} \text{ m}^{-2}$ for IPS-W, and $0.22 \times 10^{20} \text{ m}^{-2}$ for VSP-W. The samples were heated to 1200 K 5–10 min after the end of ion implantation and measurement of re-emission. In the temperature range 300–1100 K the heating rate was $4.6 \pm 0.4 \text{ K/s}$. Desorbed HD and D_2 particles were detected with a quadrupole mass spectrometer. 1–2 days after the re-emission measurements, the areas implanted at 300 K were analyzed using the D (^3He , p) α nuclear reaction (NRA) with 790 keV ^3He ion beam to determine the amount of retained deuterium within the limit of sensitivity of the NRA method which was approximately 0.7 μm . The fraction of deuterium emitted as HD molecules depended mainly on the target temperature and did not exceed 0.10–0.12 at 300 K, 0.15–0.20 at 600 K, and 0.21–0.24 at 900 K.

Deuterium retention varied from a low of $2 \times 10^{19} \text{ m}^{-2}$ for the CVD and single crystal samples at 900 K up to a high of $4.5 \times 10^{21} \text{ m}^{-2}$ for the hot-rolled material at 300 K. The re-emission approached unity most rapidly for the higher

temperatures and for the single crystals. The thermal desorption spectra for the different materials were very different. TDS spectra of deuterium from W samples implanted at 300 K at fluences Φ^{sat} for single crystal W, CVD-W and IPS-W samples were characterized by a broad temperature range of release, which could be explained by the superposition of two peaks with $T_{\text{max}} \approx 400$ K and $T_{\text{max}} \approx 690$ K respectively in the W crystal and with $T_{\text{max}} \approx 400$ K and $T_{\text{max}} \approx 590$ K for CVD-W and IPS-W. The thermal release from hot-rolled W showed a broad distribution, with maximum at $T_{\text{max}} \approx 530$ K and gradual decrease between 700 K and 1000 K. VPS-W had a sharp thermal release peak at $T_{\text{max}} \approx 350$ K, small desorption steps occurred at $T_{\text{max}} \approx 500$ K and $T_{\text{max}} \approx 600$ K and a small additional peak at $T_{\text{max}} \approx 950$ K.

Most of the implanted D seemed to be strongly trapped by defects such as vacancies or cavities that already exist initially or were created during implantation. The average concentration of D atoms in the radiation induced defects was estimated to be ≤ 0.1 D/W atomic ratio. However, most of the deuterium trapped in W samples during implantation was located far beyond the ion range. The authors suggested that some of the implanted D trapped in experiments in ion-induced vacancy type defects. Apparently, another part of the implanted D diffused into the bulk and was trapped by lattice imperfections (small cavities, impurity inclusions, etc.). The TDS spectrum peak at $T_{\text{max}} \approx 950$ K observed for VPS-W could be attributed to the release of chemisorbed atomic deuterium inside the cavities.

Bizyukov et al. investigated the influence of D^+ ion irradiation on erosion, mechanical stress, and deuterium retention in tungsten films by weight loss measurements and using ion-beam methods of analysis such as Rutherford back scattering (RBS) and nuclear reaction analysis (NRA) [28]. Tungsten films 200 nm thick were deposited on polished pyrolytic graphite with an intermediate 400 nm thick copper layer. The Cu/W interface with a sharp transition between the two materials provided good depth resolution for the RBS analysis. Copper did not form carbides and did not form an alloy with W. The metal films were MS deposited in an argon atmosphere. To minimize oxygen contamination of the deposited films, the residual pressure in the chamber was $\sim 10^{-5}$ Pa. The influence of irradiation with 9 keV D_3^+ ions at the flux density of $5 \times 10^{19} \text{ m}^{-2} \cdot \text{s}^{-1}$ was studied. Erosion of W coatings was studied at fluences in the range $(0.25-7) \times 10^{23} \text{ m}^{-2}$, measuring the decrease of the W layer thickness by RBS with ^4He ions. The authors analyzed trapping of deuterium in W films measuring the depth profile of the deuterium atomic concentration. The concentration D increased to $C \approx 10$ at. % just under the surface, D enriched zone extended to a depth of 70 nm, after that the concentration slowly decreased towards the W/Cu interface. After fluences above $2.2 \times 10^{23} \text{ m}^{-2}$ the SEM studies showed on the surface of the W films the formation and growth of blisters with a diameter from 5 μm to 50 μm . The blisters formed as a result of the detachment of the W layer at the W/Cu interface. At fluences well below $2 \times 10^{22} \text{ m}^{-2}$, the bubbles covered the main part of the irradiation spot. The authors concluded that W films represented an acceptable replacement of bulk tungsten in plasma-wall interaction experiments with significantly better diagnostic accessibility.

Oya et al. consider VPS-W on an F82H (Fe-8Cr-2W) substrate as a promising plasma-facing material [39]. The F82H substrate, developed by JAEA, had low activation. Tungsten powder was melted and sprayed on the substrate by an argon and hydrogen plasma jet in a vacuum chamber. The 1 mm thick VPS-W coating was produced by TOCALO Co. Ltd. in Japan at 873 K to prevent the F82H phase transition. The density of the VPS-W coatings reached 88% of pure tungsten. Sample surfaces were mechanically polished to a mirror finish and cleaned in an ultrasonic bath. The accumulation of deuterium in the VPS-W/F82H samples was realized by two different methods: by exposure to primary D^+ ions of plasma and by implantation of accelerated D_2^+ ions. During the exposure to D-plasma, the energy and flux of D^+ ions were respectively ~ 100 eV and $\sim 1 \times 10^{22} \text{ m}^{-2} \cdot \text{s}^{-1}$. The fluence was $6 \times 10^{25} \text{ m}^{-2}$. The sample temperature was 453 K. Then the sample was cooled to room temperature during 30 min. In a few minutes after the sample was transferred to the thermal desorption spectrometry device. TDS was done from room temperature to 773 K at the heating rate of 10 K/min.

3.0 keV D_2^+ was implanted into VPS-W/F82H with the flux of $1 \times 10^{18} \text{ m}^{-2} \cdot \text{s}^{-1}$ up to the fluence $\sim 1 \times 10^{22} \text{ m}^{-2}$ at room temperature in Shizuoka University. After D_2^+ ions implantation, the sample was transferred to the TDS chamber without exposure to air. TDS was done at a heating rate of $\alpha = 0.5$ K/s to 1173 K. Surface morphology was observed with an optical microscope before and after exposure to D-plasma and after TDS. The cross section of the near-surface region of the sample was observed by scanning electron microscopy and transmission electron microscopy with the focused ion beam (FIB). The cross-sectional image of VPS-W/F82H showed that most of the tungsten grains were columnar with dimensions of 1 $\mu\text{m} \times 0.5 \mu\text{m}$. In addition, a porous structure was found around the grain boundaries and on the interface of the VPS-W layers. It was ascertained that the retention of deuterium for polished VPS-W/F82H after exposure to plasma was lower than for polycrystalline tungsten (see Figure 4).

SEM/TEM observation indicated that porous structure around the grain boundaries and interface between VPS-W layers would be a potential D desorption path, leading to the low D retention. In the case of D_2^+ ion implantation, the shape of D_2 TDS spectra was nearly identical to that for plasma-exposed VPS-W/F82H, but the amount of D_2 was quite higher for unpolished VPS-W/F82H, indicating that most of D was trapped by the oxide layer produced during VPS. Reduction of surface area via the polishing process also reduces D retention for VPS-W/F82H. Controlling the chemical states of the surface was important in reducing tritium retention for materials used in future fusion devices.

Niu et al. studied the chemical states and deuterium retention behavior in VPS-W coatings and elucidate the mechanism of interaction between deuterium and tungsten coatings [40]. Tungsten coatings about 300 μm thickness were prepared on copper alloy substrates using a vacuum plasma spraying system (A-2000, Sulzer Metco, Switzerland). Argon and hydrogen were used as plasma source gases. Tungsten coatings had the original (un-polished) or polished surface.

The test setup consisted of two vacuum chambers. One of them was equipped with thermal desorption spectroscopy and a deuterium ion gun, and the other was equipped with X-ray photoelectron spectroscopy (XPS) (ESCA 1800 series, manufactured by ULVAC PHI Inc.). The Al K α was used for X-ray source. Both chambers were connected to each other via a gate valve. The sample was mounted on the holder with a ceramic heater. To remove gaseous impurities such as H₂O, O₂, and H₂, both chambers were evacuated to a vacuum of less than 10⁻⁷ Pa using ion pumps, and then the sample was preheated at 1173 K for 10 min under ultrahigh vacuum. The XPS measurements were carried out after the heat-treatment.

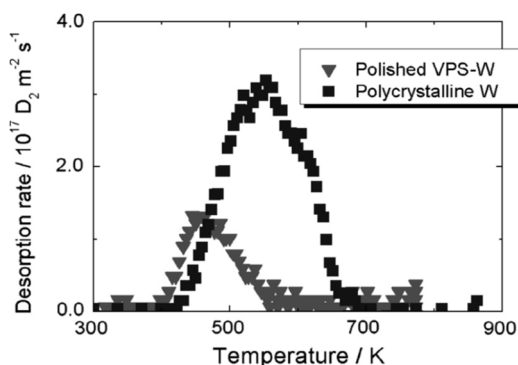


Figure 4. TDS spectra of deuterium for the D plasma-exposed VPS-W/F82H and polycrystalline W: $\alpha = 0.5$ K/s [39]

One keV D₂⁺ ions were implanted into samples at room temperature with the flux of $1.0 \times 10^{18} \text{ m}^{-2} \cdot \text{s}^{-1}$ and fluence up to $1.0 \times 10^{22} \text{ m}^{-2}$. To study the thermal desorption behavior of implanted deuterium, TDS experiments were carried out after the implantation by heating the samples up to 1150 K at the heating rate of 0.5 K/s. The desorbed gases were analyzed with a quadrupole mass spectrometer. The XPS measurements were also carried out after D₂⁺ implantation to characterize the chemical structure change. The XPS results of the original samples showed that both chemisorbed oxygen (in the O-O bond configuration) and chemical reacted oxygen (in the W-O bond configuration) existed on the surface and inside the tungsten coatings. The amount of chemisorbed oxygen inside the coating was much less compared to its amount on the surface of the coating. The chemical states of oxygen in tungsten coatings did not change after D₂⁺ implantation. But the implantation process reduced the oxygen content in the coatings due to chemical sputtering. The results of TDS of D₂ for tungsten coatings with the original and polished surfaces showed that gas was mainly desorbed in two temperature intervals ranging from 300 to 700 K and from 800 to 1150 K, respectively. For bulk W irradiated with 3 keV D₂⁺, the deuterium desorption peak located at 300–700 K, was also observed, which corresponded to the deuterium thermodesorption from intrinsic and ion-induced defects, and there was no desorption peak at higher temperatures of 800–1150 K (see Figure 5a)).

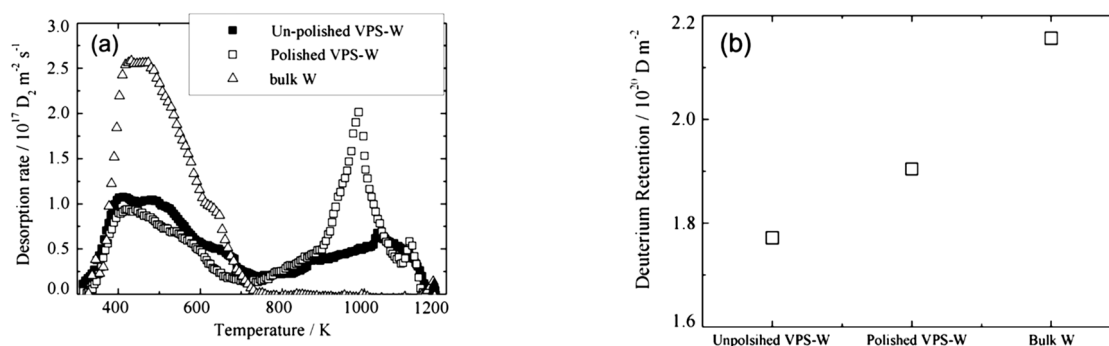


Figure 5. (a) TDS spectra of deuterium for D₂⁺ implanted W coating and bulk W and (b) comparison of deuterium retention data obtained from current TDS experiments: $\alpha = 0.5$ K/s [40]

It was considered that the deuterium desorption peak at higher temperature of 800–1150 K was due to the deuterium interaction with an oxygen impurity. The concentration C of deuterium trapping in W coatings was lower than in bulk tungsten, for which $C = 2.15 \times 10^{20} \text{ m}^{-2}$ and the trapping coefficient $\eta = 0.022$. The C and η values were: for the polished sample $C = 1.9 \times 10^{20} \text{ m}^{-2}$ and $\eta = 0.019$, and for unpolished one $C = 1.8 \times 10^{20} \text{ m}^{-2}$ and $\eta = 0.018$. The authors explained this difference in the results by the presence of oxygen in the W coatings (see Figure 5b)).

Zhang et al. analyzed 99.95% pure W films about 800–900 nm thick, deposited by magnetron sputtering on various substrates, including quartz, silicon, graphite and copper [41]. The effect of hydrogen plasma irradiation of the thin films was investigated. The samples were exposed to 50 keV hydrogen ion beam for different fluences from $2 \times 10^{21} \text{ m}^{-2}$ to $2 \times 10^{23} \text{ m}^{-2}$. The surface structure and morphology of post-irradiated samples were studied by XRD and SEM. W films, deposited on copper, crystallized after annealing at 1100 K for 1 h. When the hydrogen fluence reached $2 \times 10^{23} \text{ m}^{-2}$, on the surface of W films on copper substrates bubbles were observed, which could be caused by diffusion and retention of hydrogen at the interface between the film and substrate.

Anderl et al. reported studies of hydrogen penetration in samples of bulk tungsten and tungsten coatings on copper substrates both irradiated with a beam of 3 keV D^+ ions at a flux density of $(4-5) \times 10^{19} \text{ m}^{-2} \cdot \text{s}^{-1}$ [42]. The experiments included measurements of the re-emission and penetration rates of deuterium at temperatures from 638 K to 825 K. The time dependences of re-emission and penetration of deuterium into the sample were measured using a quadrupole mass spectrometer calibrated with deuterium standard leaks. Twenty-five-mm diameter discs of copper, tungsten, and copper with a tungsten coating were investigated in this work. Copper specimens were machined to a thickness of 0.5 mm from high-purity OFHC copper rod, and they were polished to a mirror finish using conventional metallurgical techniques. Tungsten specimens were punched from high-purity foil material (99.95% W, reduction-rolled, powder-metallurgy product) with thicknesses of 25 μm and 50 μm . The tungsten-coated copper specimen was made by sputter-deposition of a 0.5 μm thick tungsten layer onto a polished 0.5 mm thick copper disk heated to 773 K during the coating process.

From measurements, diffusion constants and surface recombination coefficients were obtained. The authors draw the following conclusions. A coating of a low solubility material (W) deposited on a higher solubility material (Cu) should result in a step increase in the deuterium concentration across the interface and lead to higher permeation than in samples of comparable thickness with uniformly high solubility. Therefore, coatings of materials with high rather than low solubility could be effective in reducing permeability.

Ogorodnikova et al. studied deuterium retention in different tungsten coatings on carbon substrates for various incident ion energies ranging from 20 eV to 200 eV per deuterium atom and fluences in the range from $1 \times 10^{23} \text{ m}^{-2}$ to $2 \times 10^{25} \text{ m}^{-2}$ [43]. The targets were irradiated with deuterium ions at the IPP laboratory by the mass-separated beam with the flux of $10^{15} \text{ m}^{-2} \cdot \text{s}^{-1}$ as well as with deuterium plasma providing the flux of $10^{16} \text{ m}^{-2} \cdot \text{s}^{-1}$. Irradiation was done at various sample temperatures from 320 K to 650 K. The depth profiles of deuterium in the W coatings were measured up to the depth of 6 μm using nuclear reaction analysis (NRA), and the total amounts of retained deuterium were determined by thermal desorption spectroscopy. It was shown that deuterium retention significantly depended on the microstructure of each W coating. The retention of deuterium in the 7 μm thick W coating produced by the CMSII method was higher compared to the 4–5 μm thick PVD-W coating and the 200 μm thick VPS-W coating for all investigated energies and sample temperatures up to 650 K.

Katayama et al. prepared tungsten coatings on W substrates at 294 K and 773 K by hydrogen radio-frequency (RF) plasma sputtering of W targets [44]. The thickness and density of the W coatings were 970 nm and 10 kg/m^3 on average, respectively. The porosity of the coatings was 0.45. In EDX analysis, no oxygen signal was detected from them. Samples were irradiated with 1 keV D^+ (2 keV D_2^+) ions to the fluence of $2 \times 10^{21} \text{ m}^{-2}$ at 294 K or 773 K. Two samples (W coatings on W substrates) and the W substrate for comparison were picked out for irradiation. Each sample was cut in half together with substrates. One of them was irradiated with deuterium ions and then analyzed by TDS. Another one was tested by TDS without exposure to deuterium ions. In both experiments, the temperature increased to 1273 K at a rate of 1 K/s. The D_2 thermal desorption rate was calibrated by a standard helium leak, taking into account the relative ionization cross section. The temperature dependences of deuterium retention in different types of samples were studied.

On the surface of W coatings deposited at substrate temperatures of 294 K and 773 K, blisters of the size from 5 μm to 15 μm were observed both before and after irradiation with 1 keV D^+ ions to the fluence of $2.0 \times 10^{21} \text{ m}^{-2}$. The cross section observation showed that the formation of blisters took place not at the boundary between the W coating and the substrate, but inside the coating. Blister formation suggested that hydrogen was implanted into the growing surface with high flux and migrated into the deeper region and gathered in voids. The blisters were ruptured after TDS of D_2 from samples.

The results of HD and D_2 release from W coatings irradiated with D^+ ions were as follows. From the W coating irradiated at 294 K D_2 release started at 320 K, while the release of HD started at 340 K, and a large peak of D_2 release was observed at 330 K. For W coating irradiated at 573 K deuterium release started at 420 K and continued up to 1130 K with the peak at the temperature of about 570 K, that corresponded to the irradiation temperature. A small peak at 1090 K was due to the release of deuterium from broken blisters. From the W coating irradiated at 773 K, deuterium released in the temperature range from 540 K to 970 K, and the peak had maximum at $T_{\text{max}} = 840 \text{ K}$. The tiny peak at 1120 K was supposed to be the result of the deuterium release from broken blisters. The deuterium retention (D/W ratio) was 0.0031 for 294 K, 0.0021 for 573 K, and 0.0004 for 773 K, i.e. decreased with increasing sample temperature during irradiation. The decrease in D/W with T increasing from 294 K to 573 K was lower than at increasing from 573 K to 773 K, although the deuterium trapping capacity at 294 K was greater than at 573 K. This was because deuterium, implanted at 294 K, was trapped only in a narrow region near the surface. It was considered that deuterium implanted at 573 K and 773 K penetrated deeper into the coatings and remained in the trap sites at both temperatures.

At heating the W coatings, both non-irradiated and irradiated at 294 K with deuterium ions, hydrogen release was observed. The ratio H/W was 0.073 for the unirradiated coating and H/W = 0.11 for the irradiated coating. During irradiation of the W coating at 773 K, part of hydrogen was released, and the H/W value was 0.05 instead of H/W = 0.11. The peak of release at the temperature of about 1100 K was explained by the rupture of blisters. The amount of hydrogen released at the temperature of about 1100 K from the irradiated sample was greater than from the unirradiated one. This indicated that hydrogen migrated in the coating during irradiation or during TDS measurement, and part of the hydrogen entered into the blister. The D/W ratio at ion irradiation under existing conditions was significantly less than H/W during the sputtering-deposition of W coating. Authors considered that this was due to the fact that the fluence of hydrogen ions in the process of sputtering-deposition was much greater than the fluence of deuterium ions in the process of D^+ ions irradiation.

The results of the HD and D₂ release from the W foil (substrate) irradiated with D⁺ ions were as follows. The deuterium signals (HD and D₂) from the W foil irradiated at 773 K were below the detection limit. From the W foil irradiated at 294 K, relatively large HD and D₂ peaks were observed at 470 K and 480 K, respectively. From the W foil irradiated at 573 K, the release of HD began at 460 K and two peaks were observed at 1020 K and 1150 K. The trapping of deuterium in the W coating irradiated at 294 K was 2.8 times greater than in the W foil. The deuterium retention in the W coating irradiated at 573 K was 17.3 times greater than in the W foil.

This work authors Bobkov et al. studied tungsten coatings of different thicknesses deposited on stainless steel substrates [36, 37, 45–49]. The stainless steel substrate 0.8 mm thick had the following composition (at%): 20 Cr, 70 Fe, 8.5 Ni, and 1.5 Ti. W coatings were irradiated with D⁺ ions to different fluences and at different temperatures of the bombarded target. Coatings were MS deposited by sputtering W target in Ar atmosphere at the pressure of 1.0 Pa on substrate at $T = 600$ K at the rate of $0.6 \text{ nm}\cdot\text{s}^{-1}$ with Ti layer less than 10 nm thick pre-deposited on it. In some cases, stainless steel substrate with Ti sublayer up to 10 nm thick was additionally coated with 3 μm thick Cu sublayer, then again Ti sublayer less than 10 nm thick, and then W layer. The thicknesses of the W coatings were or in the range of 0.1–1.0 μm or 2.2 μm . The deposition technique was described in detail in [35]. The structure, surface morphology, macrostresses of W coatings and radiation damages formed in them were studied with electron microscopy, X-ray diffractometry and thermal desorption spectrometry. The W coatings had a polycrystalline bcc structure with an average grain size from 20 nm to 60 nm. This was the nanocrystalline grain size for W, as it did not exceed 100 nm. The W coatings had different internal macrostresses depending on the thicknesses of the tungsten coatings and the multilayer nature of the substrates. They could be compressive as well as tensile. There was tensile macro stress $\sigma = +0.64$ GPa in the compositions (SSt. + Cu + W (2.2 μm)). Compressive macrostress $\sigma = -4.5$ GPa was in (SSt. + Cu + W (0.5 μm)). In the compositions (SSt. + W (2.2 μm)) and (SSt. + W (0.5 μm)) there were macrostresses $\sigma = -8.0$ GPa and $\sigma = -10.0$ GPa respectively. The copper sublayer reduced internal compressive stresses. In the listed works [36, 37, 45–49], the authors studied the types of formed radiation defects, their relationship with defects in the tungsten crystal lattice, mechanisms of their migration and annealing, including release of implanted deuterium from the sample into vacuum. Spectra of deuterium thermal desorption were analyzed and temperature intervals for the release of D₂ from the coatings into vacuum were cleared. Concentrations and trapping coefficients of implanted deuterium in coatings were determined. Changes in the microstructure of the W coatings and the morphology of their surface in the result of ion irradiation and subsequent heating were observed. To clarify the radiation stability of the system “W-film-implanted deuterium”, we studied the influence of coating thickness [45, 46, 48], the type of composite system (determined by the multilayer nature of the substrate) [45, 46], fluences of D⁺ ions irradiation [46, 47, 49] and sample temperature during bombardment [36, 37] on the above parameters, characteristics, physical and structural properties of the coatings.

The processes of implanted deuterium trapping, retention and thermal desorption, formation and annealing of radiation defects in the crystal lattice of W coatings irradiated with 5.0 keV and 10 keV D⁺ ions at flux densities of $3.0 \times 10^{16} \text{ m}^{-2}\cdot\text{s}^{-1}$ and $3.0 \times 10^{17} \text{ m}^{-2}\cdot\text{s}^{-1}$ were studied [45–49]. Fluences of ions irradiation Φ were from $0.05 \times 10^{22} \text{ m}^{-2}$ to $1.65 \times 10^{22} \text{ m}^{-2}$ and the samples were at room temperature ($T_0 = 290$ K) during the bombardment. Tungsten coatings with thicknesses from 0.1 μm to 2.2 μm were deposited on stainless steel substrates both with an intermediate copper layer (SSt. + Cu + W) and without it (SSt. + W). The influence of the W coating thickness, the type of composite system, and the fluence of D⁺ ions irradiation on the behavior of spectra of D₂ thermal desorption into vacuum were investigated. The influence of these parameters on the concentration C [m^{-2}] or C [at. %] and the deuterium trapping coefficient $\eta = C/\Phi$ was also analyzed. For low fluences $\Phi \leq 0.5 \times 10^{22} \text{ m}^{-2}$, thermal desorption of deuterium from W coatings of compositions (SSt. + Cu + W (μm , nm)) and (SSt. + W (μm)) had mainly the peak with $T_{\text{max}} \approx 640$ K (see Figure 6, curves 1–6). For high fluences $0.7 \times 10^{22} < \Phi \leq 1.65 \times 10^{22} \text{ m}^{-2}$ thermal desorption of deuterium occurred with the peak with $T_{\text{max}} \approx 640$ K (80–85% D₂ was released) as well as at $T > 1000$ K with the peak with $T_{\text{max}} \approx 1400$ K (see Figure 6, curves 7, 8).

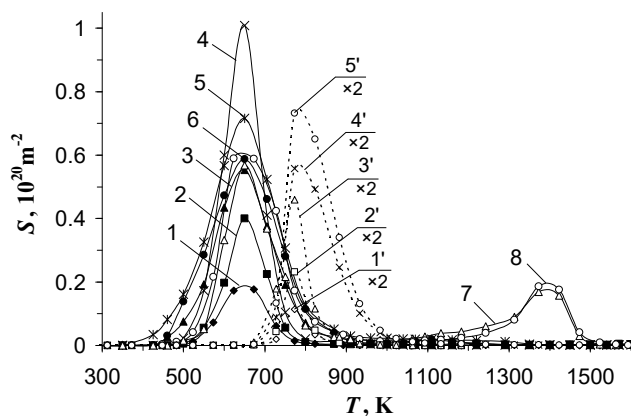


Figure 6. Thermal desorption spectra of deuterium from W (1–8) and Ta (1'–5') coatings deposited on SSt. and irradiated with 10 keV D⁺ ions to fluences $\Phi, 10^{22} \text{ m}^{-2}$: 0.1 (1, 1'), 0.2 (2, 2'), 0.3 (3), 0.4 (4, 3'), 0.5 (5), 0.7 (6), 0.8 (4'), 1.0 (7), 1.1 (5'), 1.65 (8); $T_0 = 290$ K, $\alpha = 0.8$ K/s [36, 49].

The spectra of deuterium thermal desorption from the thin W coating (SSt. + W (nm)) also had peaks of gas release in the temperature range $700 < T < 1000$ K. This was probably due to the release of deuterium into vacuum from the transition region of tungsten – stainless steel. For thin tungsten coatings with a thickness of ~ 500 nm, in both compositions (with an intermediate copper layer and without it) as the fluence increased, the concentration C of trapping deuterium increased from 0.02 at. % up to ~ 4 at. % and the deuterium trapping coefficient η increased from 0.004 to ~ 0.03 respectively. For thick tungsten coatings (with thicknesses from $1.5 \mu\text{m}$ to $2.2 \mu\text{m}$) in both compositions, with the fluence increase the concentration C increased from 0.5 at. % up to 3–4 at. %, and η decreased from (0.09–0.10) to 0.03 respectively. The authors found that at $\Phi < 1.3 \times 10^{22} \text{ m}^{-2}$ deuterium retained in higher concentrations in W (μm) coatings as compared to W (nm) coatings. With a further increase of the fluence, $1.3 \times 10^{22} < \Phi \leq 1.65 \times 10^{22} \text{ m}^{-2}$, the deuterium trapping coefficient in W (μm) coatings decreased from ~ 0.04 to 0.03, while in W(nm) coatings it increased from ~ 0.02 to 0.03.

X-ray diffraction studies of this work authors [46] showed that the initial compressive stresses in the W condensates of the studied compositions were due to the formation in W lattice its own interstitial atoms during the deposition with the used method. D^+ ions irradiation created an additional amount of defects and contributed for their radiation-stimulated migration forming clusters and complexes such as interstitial dislocation loops. Radiation defects of the vacancy type trapped and retained implanted deuterium with its subsequent release at heating from the solid solution into vacuum or into bubbles. Electron microscopic studies of W coatings [49] did not show the formation of deuterium bubbles in them at room temperature after D^+ ions irradiation up to fluences $\Phi \leq 6 \times 10^{22} \text{ m}^{-2}$. The formation of interstitial dislocation loops with average size more than 5 nm and the density $3.2 \times 10^{16} \text{ m}^{-2}$ was found out at $\Phi = 6 \times 10^{22} \text{ m}^{-2}$.

In [36, 37], effects of the samples temperature T_0 during D^+ ions irradiation on the trapping, retention, and thermal desorption of ion-implanted deuterium in vacuum, and on the formation and annealing of radiation defects in the crystal lattice of tungsten coatings were represented. The samples were irradiated with 20 keV (10 keV D^+) D_2^+ ions at the flux density of $3.0 \times 10^{17} \text{ m}^{-2} \cdot \text{s}^{-1}$. The fluences were $1.0 \times 10^{21} \text{ m}^{-2}$ and $2.0 \times 10^{21} \text{ m}^{-2}$. The temperatures T_0 were 290, 370, 440, 470, and 500 K. The thickness W of the coatings was $\sim 1.0 \mu\text{m}$. They were prepared by magnetron sputtering of a W target and deposited on a stainless steel substrate with an intermediate Ti layer pre-deposited on it. The deposition parameters and substrate temperature were the same as in [35, 45–49]. The authors noted for W coatings the influence of the samples temperature T_0 during irradiation on the behavior of the spectra of deuterium thermal desorption into vacuum, concentration C and trapping coefficient η of deuterium. The character of deuterium thermal desorption spectra retained with T_0 increasing. They had one peak of deuterium thermal desorption for all irradiated samples with the temperature T_{max} close to 640 K (see Figure 7, curves 1–5). But with the increase in temperature T_0 , the intensities of thermal desorption peaks decreased, and the start of noticeable deuterium thermal desorption from coatings shifted to the higher temperatures of post-implantation heating. As T_0 increased, the deuterium concentration and trapping coefficient η in W coatings decreased. For example, η changed from 0.06 to 0.02.

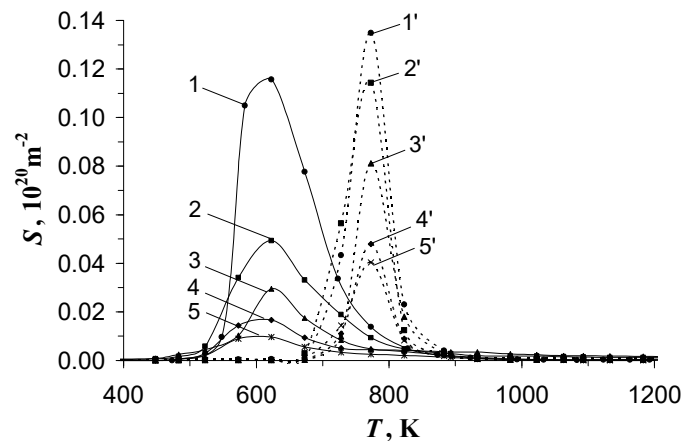


Figure 7. Thermal desorption spectra of deuterium from W (1–5) and Ta (1'–5') coatings deposited on SSt. and irradiated with 10 keV D^+ ions at different temperatures T_0 , K: 290 (1, 1'), 370 (2, 2'), 440 (3), 470 (4, 3'), 500 (5) 570 (4'), 670 (5'); $\Phi = 0.2 \times 10^{22} \text{ m}^{-2}$, $\alpha = 0.8 \text{ K/s}$ [37]

Based on the invariance of the behavior (one peak) of deuterium thermal desorption spectra for the studied temperatures T_0 of the samples and low fluences of irradiation with D^+ ions, it could be assumed that the nature of the formed radiation damages and the mechanisms of their annealing were the same. According to the results of [49], the peak of deuterium release with $T_{\text{max}} = 640$ K and with the activation energy of thermal desorption $E_a = 1.4 \text{ eV}$ was due to the dissociation of deuterium–vacancy complexes DV_n ($n = 4–10$), migration of deuterium atoms along the interstices to the surface with a migration energy $E_{\text{D}_i}^{\text{m}} \approx 0.39 \text{ eV}$, recombination into a D_2 molecule, and subsequent desorption of D_2 into vacuum. The high-temperature peak ($T_{\text{max}} \approx 1400$ K) of deuterium desorption from the W coating, observed for fluences $\Phi \geq 8.0 \times 10^{21} \text{ m}^{-2}$, was most likely due to the formation of deuterium bubbles during heating and the release of deuterium from them. Gas bubbles at such Φ were usually formed in metals at $T > 0.4 T_m$. For tungsten $0.4 T_m = 1470$ K.

It could be supposed that this peak of deuterium release was the result of the dislocations movement during the recrystallization of heated tungsten. In this experiment, it proceeded on the tail of the thermal desorption spectrum ($T > 1700$ K) and, therefore, had low effect on the release of D_2 into vacuum.

So, in tungsten coatings, D^+ ions irradiated at $T_0 = 290\text{--}500$ K, the following radiation damages, being traps for implanted deuterium, were formed: vacancy-type defects, interstitial dislocation loops, and gas-vacancy complexes. With the temperature T_0 of the samples at ion irradiation increase, as well as during subsequent post-implantation heating, thermal desorption of deuterium increased. This was due to the acceleration of the gas-vacancy complexes dissociation processes, the gas particles migration to the surface and released into vacuum.

In [10, 14, 27, 28, 36, 37, 39–49] the results of studies of the processes of trapping and retention of hydrogen isotopes in tungsten coatings were presented. The results were obtained at the implantation of accelerated D^+ , H^+ ions or plasma implantation of primary D^+ or H^+ ions. The study of the same processes in films of co-deposited hydrogen isotopes and tungsten required a separate analysis [50, 51]. These results could differ significantly from the ion implantation. Eroded particles from the plasma-facing W components (PFCs) migrated through the plasma and re-deposited on the surface in some other area of the facility while the same surface was bombarded with hydrogen isotopes from the plasma. The result of these two processes was a continuously growing co-deposited layer enriched with hydrogen isotopes. Since hydrogen accumulated in it as it grew rather than when was implanted into an already formed layer, the co-deposited films had a high hydrogen content throughout their depth. Such layers, in principle, could become rather thick, increasing with the discharge time, and could form in hard-to-reach places. All of this meant that co-deposited layers in fusion devices could store arbitrarily high amounts of hydrogen, including radioactive tritium. In tungsten layers deposited on laboratory facilities [50] the relative content D/W was 5–10 at.%. The content of hydrogen isotopes in the co-deposited layers depended on the deposition conditions: 1) – the temperature of the substrate of co-deposition, 2) – the flows of hydrogen and the re-deposited material, 3) – the energy of hydrogen particles implanting in the co-deposited layers.

Deposition conditions could vary greatly from reactor to reactor and even within the same plant. This made it important to be able to predict the content of hydrogen isotopes in co-deposited layers in the dependence on the deposition conditions, identifying areas of rapid hydrogen retention and estimating the rate of tritium retention in fusion devices.

Experimental results of tungsten and deuterium co-deposition in a wide range of substrate temperatures (from room temperature to 800 K) were presented in [50]. A simple analytical model of co-deposition based on a one-dimensional equation of diffusion with trapping was proposed. The MD-2 installation using to study the co-deposition of tungsten and deuterium had two separately evacuated chambers, a deposition chamber and a chamber for analytical thermal desorption spectrometry. A tungsten plate was sputtered by planar DC magnetron in an Ar- D_2 atmosphere. In the deposition chamber the residual pressure was less than 10^{-4} Pa, the operating pressure was 1.9 ± 0.1 Pa, and the Ar partial pressure was 0.8 Pa. The voltage, current, and discharge power were ≈ 640 V, ≈ 0.3 A, and 200 W, respectively. In the TDS chamber the residual pressure was $\sim 10^{-7}$ Pa. Tungsten-deuterium films were deposited on a molybdenum substrates. The deposition rate was ~ 0.4 nm/s. The thickness of the films deposited in each experiment was ~ 100 nm. Before placing in a vacuum, the substrate was cleaned in an ultrasonic bath with acetone and alcohol, and was annealed at ~ 1500 K for 7 h in vacuum before to the first experiment. The substrate temperatures during and after deposition were 290, 525, 600, 685, and 800 K. The substrate heating was started before deposition and turned off at the end of it. Then the substrate was cooled to room temperature in a deuterium atmosphere at a pressure of ~ 1 Pa. After that, the supply of deuterium gas was stopped, and the substrate with the co-deposited film was moved into the TDS chamber without being exposed to air. In studying the spectra of deuterium thermal desorption, the samples were linearly heated from 290 K to ~ 1450 K at the rate of 2 K/s. The release of deuterium was registered with a quadrupole mass spectrometer. The TDS spectra for D-W films, deposited at room temperature, 560 K and 800 K, included mass signals of 2, 3, 4, and 40 amu related to H_2 , HD, D_2 , and Ar. If the substrate during the deposition was at 290 K, for mass 4 the signal peaks with maxima at ~ 500 K, ~ 700 K, and ~ 1000 K were observed. If the substrates at deposition were at 290 K and 560 K, deuterium released mainly as D_2 molecules but for the films deposited at 800 K, the contributions of HD and D_2 molecules were comparable. The total deuterium concentration was ~ 5 at.% for deposition at 290 K, 2.2 at.% for 570 K, and 0.37 at.% for 800 K. When calculating the deuterium content, both D_2 and HD were taken into account. A simple analytical approach was proposed based on the assumption of a quasi-stationary equilibrium between mobile and trapping deuterium during a slow film growth. The model described the experimental data very well, supposing three types of traps for deuterium in a W-D film: D trapping on dislocations with the energy 0.74 ± 0.08 eV; trapping of several D atoms into one vacancy with the energy 1.18 ± 0.12 eV; D trapped into a vacancy with the energy 1.56 ± 0.16 eV. Trap concentrations were 2.3 at.%, 1.8 at.% and 1.0 at.% respectively.

Gasparyan et al. represented the dependence of deuterium concentration in co-deposited W-D, Mo-D, and Al-D films on the substrate temperature (from room temperature to 800 K) during the deposition (see Figure 8) [51]. The maximum D retention was in W-D films, the retention in Mo-D films was slightly lower, and the minimum value was for Al-D films. This trend contradicted the well-known tendency for solubility: W had the lowest solubility of deuterium. The decrease in the solubility of D (from Mo to W) and the increase in the total content of D in the films could be due to a higher binding energy of D with defects. Experiments with high temperature resolution revealed a characteristic step structure of the temperature dependence curve, where each step corresponded to one separate type of traps.

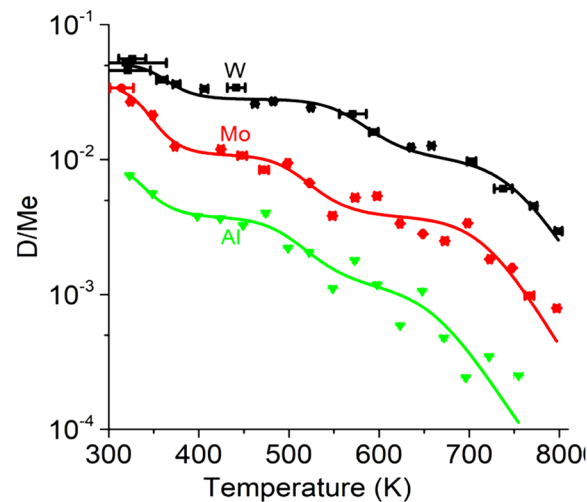


Figure 8. Dependences of deuterium concentration in atomic fractions in co-deposited W-D, Mo-D and Al-D films on the substrate temperature during deposition [51]

Helium implantation, retention and release from tungsten coatings

In the course of a nuclear fusion reaction, one of the products is helium with the energy varies from a few eV to tens of keV [52]. In fusion devices, tungsten is simultaneously or sequentially irradiated with ions of hydrogen isotopes and helium. The recent studies described above have shown that the microstructure of tungsten coatings is changed at irradiation with hydrogen isotope ions. Irradiation with He^+ ions also causes various changes in the microstructure of W, such as voids or bubbles, blisters and fluff. Yu et al. simultaneously irradiated 10 μm thick nanocrystalline tungsten films and 1.5 mm thick W plates at room temperature with 60 keV He^+ ions to the fluence of $1.0 \times 10^{22} \text{ m}^{-2}$ [5]. The average ion flux density was about $2.44 \times 10^{17} \text{ m}^{-2} \cdot \text{s}^{-1}$. The residual pressure in the irradiation chamber was $5 \times 10^{-4} \text{ Pa}$. A piece of W plate of the purity 99.95% and the density 99% purchased from Advanced Technology & Materials Co., Ltd (AT&M) was prepared by powder sintering, and then heat treatment at 1273 K for 1 h for stress relieve. The average grain size in it was about 1–5 μm , there was no preferred grain orientation. The W plate was cut into several samples of 4 mm \times 4 mm. One side was mirror polished by mechanical and electrochemical polishing. Then they were used as samples for He^+ ions irradiation and as the substrates for tungsten films.

Before irradiation and deposition of the W film, all cut plates were sequentially ultrasonic cleaned with acetone, alcohol, and deionized water for 15 min. Tungsten films with the average grain size of about 50 nm were deposited on the aforementioned W substrate by magnetron sputtering in argon atmosphere at a pressure $\sim 1 \text{ Pa}$, the residual pressure was less than $5 \times 10^{-4} \text{ Pa}$. Before the deposition of tungsten films, W substrates (purity 99.95%) were bombarded by argon plasma for 10 min to remove oxides and impurities on their surface. For enhancing adhesion and preventing the delamination of W film, the substrate during deposition was heated up to 770 K and then the temperature was kept constant for the first 2 h, and reduced to 520 K for the next 8 h. The film deposition rate was about 1 $\mu\text{m}/\text{h}$. Research methods were SEM and X-ray diffraction.

The irradiation experiments were performed at 320 keV multi-discipline research platform for Highly Charged Ions equipped with an Electron Cyclotron Resonance (ECR) plasma source in the Institute of Modern Physics, Chinese Academy of Sciences (IMP, CAS), in Lanzhou

Numerous blisters were observed after He^+ ions irradiation on the surface of both types of samples. Blisters with sizes from a few micrometers to about 20 μm were formed on the entire surface of the bulk W (see Figure 9).

On the surface of the W film, blisters of several micrometers were formed (see Figure 10). The authors noted that at the same parameters of He^+ ions irradiation, the density and average size of blisters in the bulk W were greater than in the W film. This indicated that the structure of nano-crystalline tungsten film affected the formation of blisters. In W nanostructured films, besides the ion-induced defects, the presence of initial defects, trapping implanted helium particles, was more characteristic. The latter included point defects, dislocations, vacancies, voids, and a high density of grain boundaries (GBs) which could be absorbers of implanted helium particles and displaced matrix atoms along the He^+ ion range. These facts resulted in a delay of the formation of helium bubbles with excess pressure, as well as blisters formation and W film detachment or layering.

Accounting the structural difference between bulk W and W film, the authors suggested that the formation of blisters, their rupture and detachment on the surface of bulk W should begin earlier than that in the film. As the amount of GBs in the nanocrystalline W film was greater than in the bulk W, the critical fluence of blister formation should be higher; therefore, the density of blisters on its surface was lower. In addition, in the magnetron deposited W film, there were compressive stresses that should prevent the formation of blisters caused by He^+ ions irradiation. Therefore, the blisters on the W film surface were smaller than on the surface of bulk W.

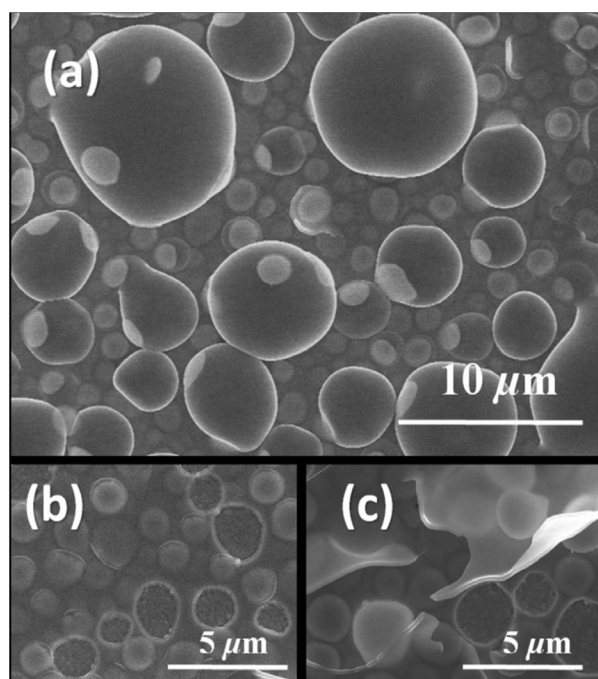


Figure 9. Blistering of the surface of bulk W: (a) big blisters with size from several to tens micrometers, (b) small blisters with size of no more than 2 μm and (c) blisters under the ruptured blisters [5]

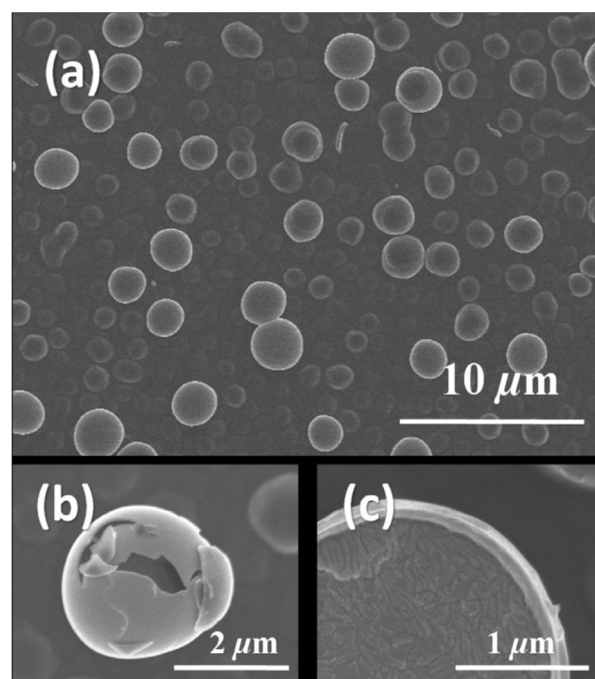


Figure 10. Blistering of the surface of W film: (a) blisters with size of several micrometers, (b) ruptured blisters and (c) surface morphology under a ruptured blister [5]

Jiang et al. proposed tungsten coatings on V-4Cr-4Ti alloy substrates [8], considering it as a promising structural material because of alloy good creep resistance, high thermal stress coefficient, and excellent corrosion resistance. Such tungsten coatings with a thickness of 500 μm were prepared by electrodeposition in a molten salt with vanadium based alloy plate (V-4Cr-4Ti, 30 mm \times 25 mm \times 5 mm, self-provided) as the cathode and pure tungsten plate (purity: 99.95%, 30 mm \times 25 mm \times 5 mm, TLWM Co., Ltd) as the anode. Na_2WO_4 and WO_3 (99.5%, Tianjin Fu Chen Chemical Reagents Factory) were dried in a furnace at 773 K for 24 h. The dried chemicals were well mixed into a eutectic composition ($\text{Na}_2\text{WO}_4:\text{WO}_3 = 0.6:0.2$, by mole ratio) and then melt in an electric furnace at 1173 K. Prior to electrodeposition, the electrode surfaces were mechanically polished to obtain high quality surfaces and then cleaned in acetone and distilled water by ultrasonic cleaning. Tungsten coating was electrodeposited on V-4Cr-4Ti alloy substrate from the molten salt in an open bath at the temperature of 1173 K.

Surface SEM micrographs of tungsten coatings were obtained after irradiation with 10 keV He^+ or 65 keV He^+ ions at different fluence. At the fluence of $2.67 \times 10^{20} \text{ m}^{-2}$, the change in the surface morphology of the W coatings was relatively small, while at the fluence of $2.67 \times 10^{22} \text{ m}^{-2}$, small folded defects were visible. At the fluence of $2.67 \times 10^{20} \text{ m}^{-2}$ of 65 keV He^+ ions needle-like pores were noticeable on the surface of W coatings, and at the fluence of $2.67 \times 10^{22} \text{ m}^{-2}$ broken helium bubbles were observed.

This work authors in [37, 47, 49, 53, 54] studied effects of He^+ ions irradiation on tungsten coatings deposited on stainless steel substrates. The substrate 0.5 mm thick had the following composition: 20 Cr, 70 Fe, 8.5 Ni, and 1.5 Ti at %. The W coatings were irradiated with He^+ ions to different fluences [47, 49, 54] and at different temperatures of bombarded target [37, 53]. Processes of trapping, retention, and thermal desorption of implanted helium, as well as the formation and annealing of radiation defects in the crystal lattice of W coatings irradiated with 10 keV He^+ ions at the flux density of $3.0 \times 10^{17} \text{ m}^{-2} \cdot \text{s}^{-1}$, were studied [47, 49]. Fluences of ions irradiation Φ were from $0.05 \times 10^{22} \text{ m}^{-2}$ to $5.2 \times 10^{22} \text{ m}^{-2}$. The samples were at room temperature during the bombardment. Tungsten coatings were deposited by magnetron sputtering of a W target in an Ar atmosphere at the pressure ~ 1.0 Pa. The deposition rate and substrate temperature were the same as in [35–37, 45–46, 48]. The W deposition was done according to two schemes: 1) on stainless steel (SSt.) substrate coated with Ti less than 10 nm thick (SSt. + W); 2) on SSt. with Ti sublayer, then coated with 3 μm thick Cu layer, Ti sublayer and W deposition after that (SSt. + Cu + W). The tungsten coatings thickness was 2.2 μm . They had a polycrystalline structure with an average grain size of about 60 nm. Tungsten coating in composition (SSt. + Cu + W) had a small tensile macrostress $\sigma = +0.64$ GPa, while in (SSt. + W) the macrostress of the tungsten coating was compressive with $\sigma = -8.0$ GPa. For studying the helium retention and the formation of radiation damages in the crystal lattice of tungsten coatings, TDS, electron microscopy, and X-ray diffractometry, described in detail in [37, 45–47, 49, 54], were used. We studied the influence of He^+ ions fluence on the character of spectra of the helium thermal desorption from W coatings of the named composite systems. It was shown that the type of the composite system under study practically had no effect on the form of helium thermal desorption spectra. For W coatings at low fluences $\Phi \leq 0.4 \times 10^{22} \text{ m}^{-2}$, helium released into vacuum in the temperature range $700 \leq \Delta T \leq 1750$ K. In He TDS spectra from

coatings, the authors observed one predominant helium thermal desorption peak with $T_{\max} \approx 1520$ K and 100% helium release into a vacuum. When coatings were irradiated to high fluences of $0.47 \times 10^{22} \leq \Phi \leq 5.2 \times 10^{22} \text{ m}^{-2}$, helium TDS spectra in addition had also another region of He release, located in the temperature range 450–1300 K. With the Φ increase the fraction of helium in it grew to (65–70) % (see Figure 11a).

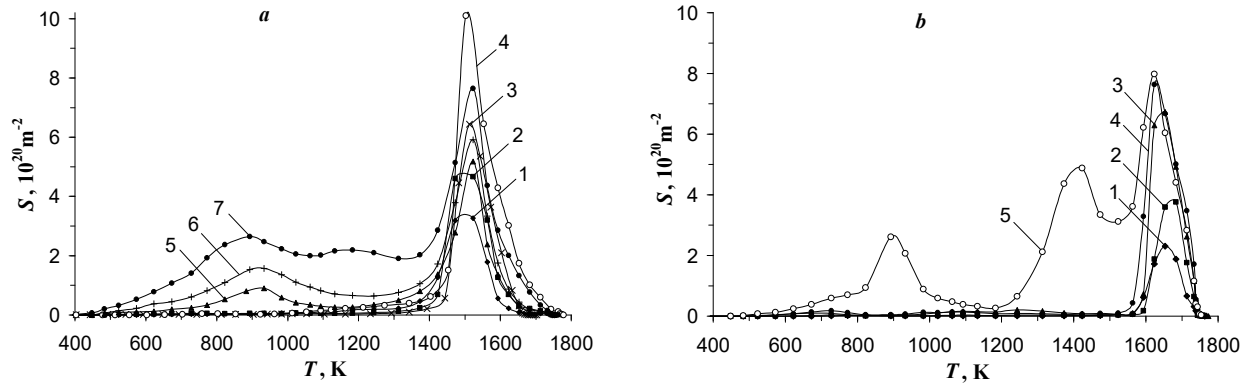


Figure 11. Thermal desorption spectra of helium from W (a) and Ta (b) coatings deposited on SSt. substrates and irradiated with 20 keV He^+ ions. Fluences Φ , 10^{22} m^{-2} : 0.1 (1), 0.2 (2), 0.31 (3), 0.4 (4), 0.47 (5), 0.61 (6), 0.83 (7) for W; 0.1 (1), 0.2 (2), 0.4 (3), 0.6 (4), 1.0 (5) for Ta; $T_0 = 290$ K, $\alpha = 0.8$ K/s [53]

The studies of microstructure of W coatings with helium implanted at the temperature $T_0 \approx 290$ K [37, 47, 49, 54] showed that at fluences of He^+ ions irradiation $\Phi < 7.0 \times 10^{21} \text{ m}^{-2}$, the interstitial dislocation loops with the density of $3.2 \times 10^{16} \text{ m}^{-2}$ and the average size more than 5 nm and dislocation networks formed. At this, the formation of helium bubbles was not observed. The formation of helium bubbles was detected after He^+ ions irradiation up to fluences $\Phi \geq 7 \times 10^{21} \text{ m}^{-2}$. They had the average diameter of about 2.5 nm and the density of $\sim 5 \times 10^{16} \text{ m}^{-2}$ at $\Phi = 7 \times 10^{21} \text{ m}^{-2}$.

The influence of the samples temperature T_0 during He^+ ions irradiation to various fluences on the trapping, retention, and thermal desorption of ion-implanted helium in vacuum, and the formation and annealing of radiation defects in the crystal lattice of tungsten coatings was shown in [37, 53]. The thickness of W coatings was $\sim 1.0 \mu\text{m}$. They were prepared by magnetron sputtering of a W target in an Ar atmosphere at a pressure ~ 1.0 Pa and deposited on a stainless steel substrate 0.8 mm thick with pre-deposited the intermediate Ti layer less than 10 nm thick. The way of preparation, deposition rate and substrate temperature were the same as in works [35–37, 45–49]. The samples were irradiated by 20 keV He^+ ions at the flux density of $3.0 \times 10^{17} \text{ m}^{-2} \cdot \text{s}^{-1}$. Fluences varied in the range $0.1 \times 10^{22} < \Phi \leq 1.0 \times 10^{22} \text{ m}^{-2}$. The samples temperatures T_0 were 290, 370, 470, 540, 570, 670, and 870 K. The effect of temperature T_0 on the helium retention and thermal desorption from the W coating into vacuum was studied for low Φ , not exceeding $0.4 \times 10^{22} \text{ m}^{-2}$, as well as for high Φ from the interval $0.47 \times 10^{22} \leq \Phi \leq 1.0 \times 10^{22} \text{ m}^{-2}$.

The character of the spectra of helium thermal desorption from tungsten coatings, He^+ ions irradiated to the same fluence from the low Φ values at different temperatures T_0 , did not changed with T_0 increasing. The spectra had one peak with the maximum at $T_{\max} \approx 1520$ K. However, with T_0 increasing, the intensity of these peaks decreased. Besides, with T_0 increase, the start of noticeable helium thermal desorption from the coatings shifted to the higher temperatures of post-implantation heating.

When W coatings irradiated with He^+ ions to a fluence $\Phi \sim 7.0 \times 10^{21} \text{ m}^{-2}$ from the high values, the thermal desorption spectra changes significantly with temperature T_0 increasing. Two temperatures were compared: room temperature $T_0 = 290$ K and elevated $T_0 = 570$ K. As noted above [47, 49], at room temperature helium TDS spectra from the coating had both the main region of helium release in the peak with $T_{\max} \approx 1520$ K and another region of its release in the temperature range 450–1300 K. At the elevated temperature, the thermal desorption spectra contained only one main peak at $T_{\max} \approx 1520$ K. No change in the peak height with increasing temperature T_0 was observed.

The regularities of helium retention in tungsten coatings of two types of composite systems at room temperature [47, 49] were analyzed based on the dependences of helium concentration C and trapping coefficient η on the fluence of He^+ ion irradiation of the samples. The increase of Φ resulted in C increase and η decrease. For example, the value of η ($\pm 10\%$) decreased from 0.8 to 0.2 with Φ increasing in the range $0.1 \times 10^{22} \leq \Phi \leq 3.55 \times 10^{22} \text{ m}^{-2}$. Dependences $C, \eta = f(\Phi)$ at $\Phi \geq 1.5 \times 10^{22} \text{ m}^{-2}$ tended to saturation, which could be associated with increasing the amount of implanted He^+ that released from the samples during ion bombardment. The values of helium C and η for the W coating in the composite system SSt. + W(μm) was slightly higher than the analogous C and η values for the composite system SSt. + Cu + W(μm). Early the difference between the type of macrostresses in the tungsten coating of these two composite systems was noted. Perhaps this fact could explain the observed discrepancy between the C and η values for helium. For the elevated temperature of tungsten coatings $T_0 = 570$ K, with an increase in the fluence of He^+ ions irradiation, C increased, and η ($\pm 10\%$) decreases slightly. In the range $0.1 \times 10^{22} < \Phi \leq 0.7 \times 10^{22} \text{ m}^{-2}$, η decreased from 0.82 to 0.68 at $T_0 = 290$ K and from ~ 0.60 to ~ 0.58 at $T_0 = 570$ K.

Thus, when T_0 of tungsten coatings during helium implantation increased, C decreased for both low and high values of Φ fluences. For T_0 in the interval of 290–570 K, C decreased approximately 1.6 times for low fluences and 1.2 times for high fluences; η ($\pm 10\%$) decreased from 0.82 to 0.50 for low Φ and from 0.7 to 0.6 for high Φ .

According to [49] calculations, the activation energy of helium thermal desorption peak with $T_{\max} \approx 1520$ K was $E_a \approx 4.2$ eV, which was close to the dissociation energy 4.42 eV for a helium-vacancy complex of the HeV type. The dissociation of the HeV complex included the release of He from a vacancy with the binding energy of 3.9 eV, the migration of a helium atom along interstices to the surface with the migration energy of 0.28 eV, and He desorption into vacuum. Helium thermal desorption into vacuum at $T \leq 1400$ K from the W coating, He⁺ irradiated at room temperature to high $\Phi \geq 0.47 \times 10^{22} \text{ m}^{-2}$, occurred as a result of gas release from other defects in the coating structure after the formation of helium bubbles, which were observed by the authors of this paper [47, 49].

When W coatings were high-temperature irradiated by He⁺ ions to low fluences, no effect of the temperature T_0 on the behavior of the helium TDS spectra was found. Based on the unchanging of the spectra nature (one peak with $T_{\max} \approx 1520$ K), it could be assumed that the formed radiation damage and the mechanisms of their annealing were the same. In W coatings for the studied temperature T_0 range, the following radiation damages were formed: defects of the vacancy type, helium-vacancy complexes, and interstitial dislocation loops. Thermal desorption of helium, due to the dissociation of helium-vacancy complexes, helium migration along interstices to the surface, and release into vacuum was enhanced for samples irradiated at elevated temperatures T_0 . Part of the implanted helium was released during irradiation with He⁺ ions.

The influence of temperature T_0 on the helium retention and thermal desorption from the coating was found at W coatings irradiation by He⁺ ions at high temperatures to high fluences. It should be noted in particular that the behavior of the spectra of helium thermal desorption into vacuum changed. For samples irradiated He⁺ at room temperature up to high fluences, TDS spectra had a multi-peak temperature region with $T \geq 450$ K of release. For samples irradiated at elevated temperature $T_0 = 570$ K and high fluence $\Phi \approx 7.0 \times 10^{21} \text{ m}^{-2}$ helium TDS spectra had one peak. The peak maximum temperature was $T_{\max} \approx 1520$ K. The concentration and helium trapping coefficient decreased with temperature T_0 increasing. Based on the single-peak character of the spectra of TDS helium at elevated T_0 , it could be supposed that the nature of the formed radiation damage and the mechanisms of their annealing were the same for both high and low fluences of ion irradiation. The following radiation defects also were formed: defects of the vacancy type and helium-vacancy complexes. Upon subsequent heating after implantation, helium thermal desorption from W coatings occurred as a result of dissociation of helium-vacancy complexes, migration of gas atoms along interstices to the sample surface, and release into vacuum.

Sequential and simultaneous implantations of deuterium and helium ions into tungsten coatings

The results of sequential irradiation with D⁺ and He⁺ ions of tungsten coatings deposited on a stainless steel substrate were shown by the authors of this work in [49, 55]. We studied the effect of preliminary implantation of He⁺ (or D⁺) ions on the retention of deuterium (or helium) and their thermal desorption into vacuum. Tungsten coatings with a thickness of $\sim 1 \mu\text{m}$ were MS deposited on a stainless steel substrate 0.5 mm thick with an intermediate layer of Ti less than 10 nm thick pre-sputtered onto it. The method of their preparation, deposition rate, substrate temperature, substrate composition, and other parameters of the MS method were the same as in [35–37, 45–49, 53, 54]. The tungsten coatings had a polycrystalline structure with an average grain size of about 60 nm. The samples were irradiated at room temperature sequentially with beams of 10 keV D⁺ (20 keV D₂⁺) and 20 keV He⁺ ions at the flux density of $3.0 \times 10^{17} \text{ m}^{-2} \cdot \text{s}^{-1}$ to fluences of $\Phi_{\text{D}^+} \leq 4.6 \times 10^{21} \text{ m}^{-2}$ and $\Phi_{\text{He}^+} \leq 4.0 \times 10^{21} \text{ m}^{-2}$ in order: He⁺, D⁺ or D⁺, He⁺. The average projective and total ranges of D⁺ (10 keV) and He⁺ (20 keV) ions in the W coating were about 60 nm and 160 nm, respectively, comparable for these ions and significantly less than the coatings thickness. The radiation damage profiles of the W crystal lattice, created by D⁺ and He⁺ ions, were identical and were located in the zone of the ions implantation.

For sequential irradiations with the named ions implanted in different order at the above fluences, the thermal desorption spectra of both gases were a superposition of the thermal desorption spectra of these ions implanted separately at the same fluences. The temperature intervals for the release of deuterium and helium were the same. The temperatures of the maxima of gas-release peaks in the spectra $T_{\max} = 640$ K (D₂) and $T_{\max} = 1520$ K (He) were the same for both sequential and separate implantations of D⁺ and He⁺ ions. Pre-implantation of helium up to different fluences in the range of $1.0 \times 10^{21} \text{ m}^{-2} \leq \Phi_{\text{He}^+} \leq 4.0 \times 10^{21} \text{ m}^{-2}$ did not change deuterium concentration C_{D} and trapping coefficient η_{D} . Preliminary implantation of deuterium to various fluences in the range $1.0 \times 10^{21} \text{ m}^{-2} \leq \Phi_{\text{D}^+} \leq 4.6 \times 10^{21} \text{ m}^{-2}$ also did not change C_{He} and η_{He} . Based on these facts, the authors suggested that in tungsten coatings irradiated with D⁺ and He⁺ ions both separately and sequentially, the types of formed radiation damages and the mechanisms of their annealing were the same. According to [45–49, 54, 55], in the tungsten coating irradiated with D⁺ or He⁺ ions at room temperature, radiation defects of the vacancy type were formed, which trapped deuterium or helium into gas-vacancy complexes D_mV_n or He_mV_n . The complexes transformed into gas bubbles with the increase of concentrations of implanted gases (for example, the helium bubbles formed at fluences $\Phi_{\text{He}^+} \geq 7 \times 10^{21} \text{ m}^{-2}$ [49, 54]). According to [46, 49, 54], at irradiations with D⁺ and He⁺ ions, intrinsic interstitial atoms of W lattice were formed, and their radiation-stimulated migration with the formation of clusters and complexes such as interstitial dislocation loops was observed. The main peak with $T_{\max} = 640$ K of deuterium release was due to the dissociation of deuterium-vacancy complexes, migration of deuterium atoms along interstitials to the

surface, their recombination into a molecule, and subsequent D₂ desorption into vacuum. The main peak with $T_{\max} = 1520$ K of helium thermal desorption as well resulted from the dissociation of helium-vacancy complexes, helium atoms migration along interstitials to the surface, and their subsequent desorption into vacuum. When analyzing separate and sequential implantations of D⁺ and He⁺ ions into tungsten coatings, general regularities were established: the concentration of retained deuterium in the coatings was lower compared to helium and its trapping coefficient was approximately an order of magnitude lower. The main release into vacuum of deuterium occurred at lower temperatures as compared to helium.

Ogorodnikova et al. [56] irradiated tungsten-based materials—polycrystalline PC-W and nanostructured CMSII-W coating—simultaneously with D⁺ and He⁺ ions both in the stationary mode and in a QSPA-T quasi-stationary high-current plasma gun, in which the pulse duration was 1 ms, the number of pulses varied from one to thirty. In stationary plasma impacts, the ion energy varied from 20 eV to 3 keV, and the ion fluxes were from 10^{17} to 10^{21} m⁻² s⁻¹. The ion fluencies were 10^{20} – 10^{25} m⁻² and the target temperatures were in the range 300–1200 K. Deuterium and helium retention in the irradiated samples was measured by thermal desorption spectroscopy using a high resolution quadrupole mass spectrometer to separate the He and D₂ signals. The amount of trapping D (ion energy 20 eV, fluence 2×10^{25} m⁻²) in the CMSII-W coatings decreased from 4.5×10^{21} to 2.0×10^{21} m⁻² with the temperature increase from 290 K to 650 K. The retention of D in PC-W decreased with temperature increasing at low $\Phi \leq 10^{22}$ m⁻². The retention of D in PC-W at the high fluence $\Phi = 10^{25}$ m⁻² with temperature increasing firstly increased and then decreased. The amount of trapping He (ion energy 60 eV, fluence 2×10^{24} m⁻²) in the CMSII-W coating increased from 0.6×10^{20} to 4.0×10^{20} m⁻² with the increase in temperature from 290 K to 1100 K. The He retention in PC-W did not significantly depend on the sample temperature at He⁺ ion energies above 400 eV and low fluences of $\Phi \leq 10^{22}$ m⁻², whereas it increased at He⁺ ion energies below 80 eV and high fluences of 2×10^{24} m⁻².

The results of helium influence on deuterium retention in co-deposited tungsten films were shown in [57]. For co-deposition W films a tungsten target was sputtered in a magnetron discharge in an Ar-D₂-He mixture. $P_{\text{Ar}} = P_{\text{D}_2} = 2.8$ Pa, $P_{\text{He}} = 0\text{--}20\%$ P_{D_2} . The residual pressure was 3×10^{-5} Pa, deposition rate was 0.2 nm/s, thickness of the deposited films was 100 nm. The sample temperature at the deposition was varied from 300 K to 800 K, the temperature jump was 50 K. The prepared films were analyzed by thermal desorption spectroscopy; the samples were linearly heated at the rate of 2 K/s to 1250 K. He and D₂ flows in TDS analysis were separated by two quadrupole mass spectrometers. In co-deposited films, the content of D₂ increased when 5% He was in the working gas and decreased with the presence of 20% He in the working gas as compared to films deposited without helium addition. The highest content of deuterium was D/W = 0.5 at.% for 5% He at the sample temperature of 800 K. The addition of 5–20% He to the working gas suppressed D₂ desorption at high temperatures $900 < T < 1100$ K, possibly due to competition between D₂ and He for the same places of trapping. For He/D > 0, D₂ desorption at high temperatures increased with increasing the deposition temperature: the peak at 800–900 K for He/D = 5%, the peak at 700–800 K for He/D = 20%.

Implantation of deuterium and helium ions into composite structure with tantalum coating

This work authors studied the processes accompanying the implantation of D⁺ or He⁺ ions into tantalum coatings deposited on stainless steel substrates [36, 37, 53]. The trapping and retention of deuterium or helium and their thermal desorption into vacuum, formation and annealing of radiation damages in the crystal lattice were studied. The types of radiation defects were determined and their interaction with ion-implanted gases was analyzed studying gases influence on the structural and physical properties of the coatings. The radiation stability of the samples at changing both their temperature during bombardment and the fluence of ions irradiation was studied. Tantalum coatings of ~ 1.5 μm thick were prepared by magnetron sputtering of a Ta target in an Ar atmosphere at a pressure ~ 1.0 Pa. Coatings were deposited at the rate of 0.6 nm/s on the 0.8 mm thick stainless steel substrates at the temperature of 600 K. An intermediate Ti layer of less than 10 nm thickness was pre-deposited on the substrate. The deposition rate, substrate temperature, substrate composition, and parameters of the MS method were the same as in [35, 45–49, 55] for tungsten coatings. The samples were irradiated with 20 keV D₂⁺ (10 keV D⁺) or 20 keV He⁺ ions at the flux density of 3.0×10^{17} m⁻²·s⁻¹ to fluences Φ in the range $(0.1 - 1.0) \times 10^{22}$ m⁻². Ions were implanted at several sample temperatures: deuterium at $T_0 = 290, 370, 470, 570,$ and 670 K, and helium at $T_0 = 290, 370, 670, 770,$ and 870 K. The average projective and total ranges of D⁺ and He⁺ ions in the Ta coating were about 60 nm and 160 nm, respectively, were comparable for these ions and significantly less than the coating thickness. Distribution profiles of radiation damages in the Ta crystal lattice created by D⁺ and He⁺ ions were located in the zone of the ions implantation.

Thermal desorption of deuterium from tantalum coatings irradiated with D⁺ ions to different fluences in the range of $0.1 \times 10^{22} \leq \Phi \leq 1.1 \times 10^{22}$ m⁻² was studied in [36]. During the bombardment the samples were at room temperature ($T_0 = 290$ K). A noticeable release of deuterium from coatings started at temperatures $T \geq 500$ K and ended at $T \approx 1100$ K. The deuterium thermal desorption spectra had one peak, the maximum of which was at a temperature $T_{\max} \approx 770$ K (see Figure 6, curves 1'–5').

The influence of samples temperature T_0 in the range of 290–670 K during D⁺ ions irradiation up to $\Phi = 2.0 \times 10^{21}$ m⁻² on the trapping, retention, and thermal desorption of deuterium from Ta coatings into vacuum was shown in [36, 37]. The character of the deuterium TDS spectra retained with T_0 increasing. The spectra had one peak and the temperature at the peak maximum $T_{\max} \approx 770$ K (see Figure 7, curves 1'–5'). As the temperature T_0 increased, the

intensity of the D₂ thermal desorption peak decreases. In addition, the deuterium noticeable release from coatings starts at higher temperatures of post-implantation heating shifting from 500 K to 690 K.

With T_0 increase, concentration C and trapping coefficient η of deuterium decreased. For example, η changed from 0.02 to 0.005 at $\Phi = 2.0 \times 10^{21} \text{ m}^{-2}$. With an increase of the D⁺ ions fluence at a constant temperature T_0 of coatings, the concentration C of deuterium decreased. The deuterium trapping coefficient η did not change in this case, whereas in W coatings deuterium trapping coefficient decreased in similar experiments (see [36]). This could be due to the different type of deuterium solubility: endothermic (W) or exothermic (Ta) and the ability to form hydrides in tantalum. The release of deuterium with the peak maximum at $T_{\text{max}} \approx 770 \text{ K}$ and the activation energy of thermal desorption $E_a = 1.7 \text{ eV}$ [37] was explained by the dissociation of deuterium-vacancy complexes, migration of deuterium atoms along the interstitials to the surface with the migration energy $E_{D,i}^m \approx 0.39 \text{ eV}$, recombination into a D₂ molecule and subsequent desorption into vacuum.

Helium thermal desorption from tantalum coating irradiated at $T_0 = 290 \text{ K}$ with He⁺ ions to different fluences in the range $0.1 \times 10^{22} \leq \Phi \leq 1.0 \times 10^{22} \text{ m}^{-2}$ was studied in [53]. The He TDS spectra were shown in Figure 11b. For low fluences $\Phi \leq 6.0 \times 10^{21} \text{ m}^{-2}$, helium released from the coatings into vacuum in the temperature range $500 \leq \Delta T \leq 1750 \text{ K}$, with the main peak having maximum at $T_{\text{max}} \approx 1670 \text{ K}$. For the highest fluence $\Phi = 1.0 \times 10^{22} \text{ m}^{-2}$ in the helium TDS spectra another temperature range of 480–1550 K of its release appeared. According [37], the spectra of helium thermal desorption into vacuum from Ta coatings, irradiated with He⁺ ions to the same fluence $\Phi = 2.0 \times 10^{21} \text{ m}^{-2}$ from the range of low Φ , at different temperatures T_0 of the samples in the range of 290–870 K, kept their behavior with T_0 increasing. The spectra had one peak with the temperature of peak maximum $T_{\text{max}} \approx 1670 \text{ K}$.

With T_0 increase, the concentration C and the helium trapping coefficient η of Ta coatings decreased. For example, η changed from 0.8 to 0.6 at $\Phi = 2.0 \times 10^{21} \text{ m}^{-2}$. With the fluence of He⁺ ions irradiation increase for Ta coatings at $T_0 = 290 \text{ K}$, the concentration C and the helium trapping coefficient η also decreased (see [36]). In [37, 53] the authors explained the release of helium with the main peak at $T_{\text{max}} = 1670 \text{ K}$ in its thermal desorption spectra by dissociation of helium-vacancy complexes, migration of helium atoms along interstices to the surface, and their subsequent desorption into vacuum. The mechanism of thermal desorption was described in detail in [37, 49].

The authors of [36, 37, 53] for Ta or W coatings established general regularities of the processes of D₂ and He retention and thermal desorption, the formation and annealing of radiation defects in the crystal lattice, and some differences in the values of their parameters. The concentration C and trapping coefficients η_D , η_{He} of implanted gases, temperature intervals of release into vacuum, and temperature T_{max} of deuterium (helium) thermal desorption peaks for these coatings had different values.

From the above it can be concluded the following:

1. TDS spectra of deuterium (helium), whose ions are implanted in Ta or W coatings at room temperature ($T_0 = 290 \text{ K}$) and low fluences no more than $1.1 \times 10^{22} \text{ m}^{-2}$ ($0.6 \times 10^{22} \text{ m}^{-2}$) for Ta and $0.7 \times 10^{22} \text{ m}^{-2}$ ($0.4 \times 10^{22} \text{ m}^{-2}$) for W, consist of one peak. Temperatures of peak maxima are for deuterium $T_{\text{max}} \approx 770 \text{ K}$ (Ta) and $T_{\text{max}} \approx 640 \text{ K}$ (W), and for helium $T_{\text{max}} \approx 1670 \text{ K}$ (Ta) and $T_{\text{max}} \approx 1520 \text{ K}$ (W). Temperatures of peak maximum T_{max} of the deuterium (helium) release from the Ta coating are higher compared to W one. TDS spectra of deuterium (Figure 6) and helium (Figure 11) for Ta and W coatings see above.

2. TDS spectra of deuterium (helium), whose ions are implanted in Ta or W coatings at low fluences $(0.1 - 0.2) \times 10^{22} \text{ m}^{-2}$, and elevated sample temperatures $T_0 = 290 - 870 \text{ K}$, contain one peak. The temperatures of peak maxima remain for all T_0 as for deuterium ($T_{\text{max}} \approx 770 \text{ K}$ (Ta) and $T_{\text{max}} \approx 640 \text{ K}$ (W)) as for helium ($T_{\text{max}} \approx 1670 \text{ K}$ (Ta) and $T_{\text{max}} \approx 1520 \text{ K}$ (W)). TDS spectra of deuterium (Figure 7) for Ta and W coatings see above.

3. For low fluences of D⁺ and He⁺ ions, deuterium releases into vacuum at lower temperatures as comparable with helium release.

4. At high fluences $\Phi = 1.0 \times 10^{22} \text{ m}^{-2}$ (Ta) and $0.47 \times 10^{22} \leq \Phi \leq 1.0 \times 10^{22} \text{ m}^{-2}$ (W) and $T_0 = 290 \text{ K}$ in the spectra of helium thermal desorption for coatings of both metals, besides the peaks of release with $T_{\text{max}} \approx 1670 \text{ K}$ (Ta) or $T_{\text{max}} \approx 1520 \text{ K}$ (W), there are also regions of He thermal desorption at $T = 480 - 1550 \text{ K}$ for the Ta coatings and at $T = 450 - 1300 \text{ K}$ for the W coatings. For the Ta coatings, the transformation of helium thermal desorption spectra from a single-peak to a more complex dependence occurs at higher fluences of He⁺ ions irradiation ($\Phi = 1.0 \times 10^{22} \text{ m}^{-2}$ for Ta and $\Phi = 0.47 \times 10^{22} \text{ m}^{-2}$ for W).

5. At all studied D⁺ or He⁺ ions fluences and T_0 for both tantalum and tungsten coatings, the concentration C_{He} and helium trapping coefficient η_{He} are much higher than the C_D and η_D for deuterium. Deuterium retains with a trapping coefficient approximately an order of magnitude lower than helium (see Figure 12 and Figure 13).

6. When the fluence of He⁺ ions irradiation increases, η_{He} decreases in the coatings of both materials. η_D decrease with the Φ increase for D⁺ ions is observed only for tungsten coatings. For tantalum coatings η_D does not change with Φ increasing. Dependences η_D , $\eta_{He} = f(\Phi)$ for coatings of both materials irradiated with D⁺ or He⁺ ions are shown in Figure 12.

7. When the temperature T_0 of tantalum and tungsten coatings during irradiation with D⁺ (He⁺) ions increases, the trapping coefficient η_D (η_{He}) of deuterium (helium) decreases. Figure 13 shows the dependences η_D , $\eta_{He} = f(T_0)$ for coatings of both irradiated materials. Comparing the same intervals of T_0 changing, a more significant η_D decrease is observed for the tungsten coatings compared to the tantalum coatings (by about 15 times and 2 times, respectively). The η_{He} decrease for the tungsten coating is insignificant (approximately 2 times and 1.5 times, respectively) comparing to the tantalum coating.

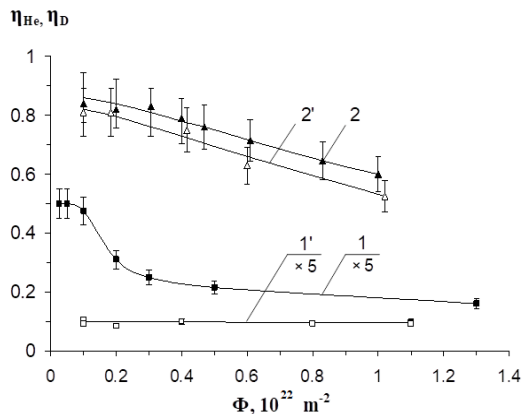


Figure 12. Deuterium (1, 1') and helium (2, 2') trapping coefficients versus the fluence of D⁺ and He⁺ ions for the W coating, curves 1, 2 and for the Ta coating, curves 1', 2'; ion energy: D⁺ – 10 keV, He⁺ – 20 keV; T₀ = 290 K [36]

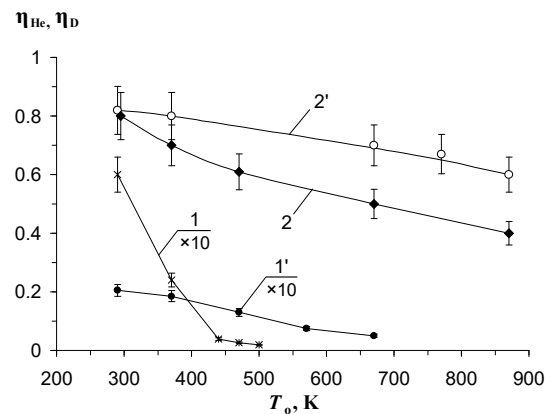


Figure 13. Deuterium (1, 1') and helium (2, 2') trapping coefficients versus temperature T₀ of the W coatings—curves 1, 2 and of the Ta coatings—curves 1', 2'. Ion energy: D⁺ – 10 keV, He⁺ – 20 keV; fluence 0.2×10²² m⁻² [37]

CONCLUSIONS

The analysis of published works about the influence of implanted hydrogen isotopes and helium on changes in the microstructure, morphology, and physical properties of tungsten and tantalum coatings, irradiated with D⁺, H⁺, and He⁺ ions, was made. The samples that irradiated both with beams of accelerated ions of hydrogen isotopes or He⁺, and in plasma containing the above-named ions were under consideration. The implantation of the above mentioned gases was performed in various modes of irradiation: individual, sequential in different order of the selected types of ions, and simultaneously with several given types of ions. Various fluences and energies of the bombarded ions were applied. The target temperature during implantation was chosen in a wide range. Modern highly sensitive research methods were used in analyzed works: electron microscopy, re-emission mass spectrometry, thermal desorption spectrometry, X-ray photoelectron spectroscopy, X-ray diffraction, analysis of nuclear reaction and Rutherford ion scattering. Simultaneous irradiation of W in bulk and in thin-film forms permitted to obtain data on the retention and migration of ion-implanted hydrogen isotopes in various types of W samples. In addition, the information about the formation of radiation damages in the crystal lattice and their interaction with the implanted gases was got. Studies of the processes of retention and release of D₂ and He, the formation and annealing of radiation defects in the crystal lattice of W and Ta coatings, carried out under similar conditions, established the common regularities of these processes in different metal coatings, as well as some differences in the parameters characterizing them. The influence of the metal choice for coatings on the concentrations and trapping coefficients of implanted gases, temperature intervals of gas release into vacuum, and temperatures of maxima T_{max} of thermal desorption peaks for deuterium (helium) into vacuum were shown.

It can be seen from this review that each presented paper contains useful information regarding the retention and release of hydrogen isotopes or helium from W and Ta coatings of plasma-facing structures for fusion reactors that needs for the efficient operation of a fusion reactor. It is necessary to take into account the radiation stability of the structural, physical and mechanical properties of promising PFM to the influence of implanted hydrogen isotopes and helium.

In the analyzed works the authors considered ways to solve one of the main problems of ITER and future tokamaks – the retention of H and He isotopes in PFC. The authors of this article, based on an analysis of the reviewed works, believe that one of the best solutions to this problem is nanocrystalline tungsten coatings deposited on reactor devices contacting with plasma.

Funding. This research did not receive any specific grant from funding agencies in the public, commercial, or not-for-profit sectors.

Conflict of Interest. Authors declared that there is no conflict of interest. The authors declare that they have no known competing financial interests or personal relationships that could have appeared to influence the work reported in this paper.

ORCID

Mykola Azarenkov, <https://orcid.org/0000-0002-4019-4933>; Lyudmila Tishchenko, <https://orcid.org/0000-0002-6300-6448>
 Valentyn V. Bobkov, <https://orcid.org/0000-0002-6772-624X>; Dmytro Shevchenko, <https://orcid.org/0000-0002-4556-039X>
 Lyubov Gamayunova, <https://orcid.org/0000-0001-7220-9944>; Anatolij Skrypnyk, <https://orcid.org/0000-0003-3691-2477>

REFERENCES

- [1] L. Pranevicius, L. Pranevicius, and D. Milcius, *Tungsten Coatings for Fusion Applications*, (Vytauto Didžiojo universitetas, Kaunas, 2009), pp. 262.
- [2] Z. Tian, J.W. Davis, and A.A. Haasz, *J. Nucl. Mater.* **399**, 101 (2010). <http://doi.org/10.1016/j.jnucmat.2010.01.007>
- [3] E.V. Kornelsen, *Canad. J. Phys.* **48**, 2812 (1970). <https://cdnsiencepub.com/doi/abs/10.1139/p70-350>
- [4] N. Yoshida, *J. Nucl. Mater.* **266-269**, 197 (1999). [https://doi.org/10.1016/s0022-3115\(98\)00817-4](https://doi.org/10.1016/s0022-3115(98)00817-4)
- [5] J. Yu, W. Han, Z. Chen, and K. Zhu, *Nucl. Mater. Energy.* **12**, 588 (2017). <https://doi.org/10.1016/j.nme.2016.10.001>

- [6] R. Behrisch, *J. Surf. Invest.: X-Ray, Synchrotron Neutron Tech.* **4**(4), 549 (2010). <https://doi.org/10.1134/S1027451010040014>
- [7] C. Ruset, E. Grigore, H. Maier, R. Neu, H. Greuner, M. Mayer, and G. Matthews, *Fusion Eng. Des.* **86**, 1677 (2011). <https://doi.org/10.1016/j.fusengdes.2011.04.031>
- [8] F. Jiang, Y. Zhang, and X. Li, *Fusion Eng. Des.* **93**, 30 (2015). <http://doi.org/10.1016/j.fusengdes.2015.02.020>
- [9] F. Brossa, G. Piatti, and M. Bardy, *J. Nucl. Mater.* **103**, 261 (1981). [https://doi.org/10.1016/0022-3115\(82\)90608-0](https://doi.org/10.1016/0022-3115(82)90608-0)
- [10] J. Yu, W. Han, Z. Lian, and K. Zhu, *Fusion Sci. Technol.* **73**, 5 (2018). <http://doi.org/10.1080/15361055.2017.1372680>
- [11] R. A. Neiser, G. R. Smolik, K. J. Hollis, and R. D. Watson, *J. Thermal Spray Technol.* **2**(4), 393 (1993). <http://doi.org/10.1007/bf02645870>
- [12] S. Boir-Lavigne, C. Moreau, and R. G. Saint-Jacques, *J. Thermal Spray Technol.* **4**(3), 261 (1995). <http://doi.org/10.1007/bf02646969>
- [13] S. Deschka, C. Garcia-Rosales, W. Hohenauer, R. Duwe, E. Gauthier, J. Linke, M. Lochter, W. Mallener, L. Plöchl, P. Rödhhammer, and A. Salito, *J. Nucl. Mater.* **233-237**, 645 (1996). [https://doi.org/10.1016/S0022-3115\(96\)00090-6](https://doi.org/10.1016/S0022-3115(96)00090-6)
- [14] C. Garcia-Rosales, P. Franzen, H. Plank, J. Roth, and E. Gauthier, *J. Nucl. Mater.* **233-237**, 803 (1996). [https://doi.org/10.1016/s0022-3115\(96\)00185-7](https://doi.org/10.1016/s0022-3115(96)00185-7)
- [15] I. Smid, M. Akiba, G. Vieider, and L. Plöchl, *J. Nucl. Mater.* **258-263**, 160 (1998). [https://doi.org/10.1016/s0022-3115\(98\)00358-4](https://doi.org/10.1016/s0022-3115(98)00358-4)
- [16] C. Ruset, E. Grigore, I. Munteanu, H. Maier, H. Greuner, C. Hopf, V. Phylipps, and G. Matthews, *Fusion Eng. Des.* **84**, 1662 (2009). <https://doi.org/10.1016/j.fusengdes.2008.11.053>
- [17] C. Ruset, E. Grigore, D. Falie, M. Gherendi, H. Maier, M. Rasinski, G. F. Matthews, and V. Zoita, *Fusion Eng. Des.* **88**, 1690 (2013). <https://doi.org/10.1016/j.fusengdes.2013.02.017>
- [18] H. Greuner, B. Boeswirth, J. Boscary, and P. McNeely, *J. Nucl. Mater.* **367**, 1444 (2007). <https://doi.org/10.1016/j.jnucmat.2007.04.004>
- [19] C. Ruset, E. Grigore, H. Maier, R. Neu, X. Li, H. Dong, R. Mitteau, and X. Courtois, *Phys. Scr.* **T128**, 171 (2007). <https://doi.org/10.1088/0031-8949/2007/t128/033>
- [20] E. Grigore, C. Ruset, K. Short, D. Hoefft, H. Dong, X. Y. Li, and T. Bell, *Surf. Coat. Technol.* **200**, 744 (2005). <https://sci-hub.st/10.1016/j.surfcoat.2005.02.118>
- [21] A. Cambe, E. Gauthier, J. M. Layet, and S. Bentivegna, *Fusion Eng. Des.* **56-57**, 331 (2001). [https://doi.org/10.1016/s0920-3796\(01\)00350-7](https://doi.org/10.1016/s0920-3796(01)00350-7)
- [22] K. Tokunaga, T. Matsubara, Y. Miyamoto, Y. Takao, N. Yoshida, N. Noda, Y. Kubota, T. Sogabe, T. Kato, and L. Plöchl, *J. Nucl. Mater.* **283-287**, 1121 (2000). [https://doi.org/10.1016/s0022-3115\(00\)00384-6](https://doi.org/10.1016/s0022-3115(00)00384-6)
- [23] L. Pranevičius, *Mater. Sci. (Medžiagotyra)*. **15**(3), 212 (2009). <https://matsc.ktu.lt/index.php/MatSc/article/view/26151>
- [24] Y. Niu, X. Zheng, H. Ji, L. Qi, C. Ding, J. Chen, and G. Luo, *Fusion Eng. Des.* **85**, 1521 (2010). <https://doi.org/10.1016/j.fusengdes.2010.04.032>
- [25] S. Tamura, K. Tokunaga, and N. Yoshida, *J. Nucl. Mater.* **313-316**, 250 (2003). [https://doi.org/10.1016/S0022-3115\(02\)01336-3](https://doi.org/10.1016/S0022-3115(02)01336-3)
- [26] D. Jihong, L. Zhengxiang, L. Gaojian, Z. Hui, and H. Chunliang, *Surf. Coat. Technol.* **198**, 169 (2005). <https://doi.org/10.1016/j.surfcoat.2004.10.130>
- [27] V. K. Alimov, and B. M. U. Scherzer, *J. Nucl. Mater.* **240**(1), 75 (1996). [https://doi.org/10.1016/S0022-3115\(96\)00442-4](https://doi.org/10.1016/S0022-3115(96)00442-4)
- [28] I. Bizyukov, K. Krieger, N. Azarenkov, S. Levchuk, and Ch. Linsmeier, *J. Nucl. Mater.* **337-339**, 965 (2005). <https://doi.org/10.1016/j.jnucmat.2004.09.048>
- [29] L. H. Taylor, and L. Green, *Fusion Eng. Des.* **32-33**, 105 (1996). [https://doi.org/10.1016/S0920-3796\(96\)00457-7](https://doi.org/10.1016/S0920-3796(96)00457-7)
- [30] L. Gladczuk, A. Patel, Ch. S. Paur, and M. Sosnowski, *Thin Solid Films.* **467**(1-2), 150 (2004). <https://doi.org/10.1016/j.tsf.2004.04.041>
- [31] K. Hieber, and N. M. Mayer, *Thin Solid Films.* **90**(1), 43 (1982). [https://doi.org/10.1016/0040-6090\(82\)90069-4](https://doi.org/10.1016/0040-6090(82)90069-4)
- [32] S. Sato, *Thin Solid Films.* **94**(4), 321 (1982). [https://doi.org/10.1016/0040-6090\(82\)90493-X](https://doi.org/10.1016/0040-6090(82)90493-X)
- [33] D. W. Face, and D. E. Prober, *J. Vac. Sci. Technol. A*, **5**, 3408 (1987). <http://doi.org/10.1116/1.574203>
- [34] G. S. Chen, P. Y. Lee, and S. T. Chen, *Thin Solid Films.* **353**, 264 (1999). [https://doi.org/10.1016/S0040-6090\(99\)00431-9](https://doi.org/10.1016/S0040-6090(99)00431-9)
- [35] S. S. Alimov, N. A. Azarenkov, V. V. Bobkov, I. I. Okseniuk, A. A. Skrypnyk, R. I. Starovoytov, and L. P. Tishchenko, *J. Kharkiv National University*, (1041), 116 (2013). <https://periodicals.karazin.ua/eejp/article/view/13520>
- [36] V. V. Bobkov, L. P. Tishchenko, Yu. I. Kovtunencko, O. B. Tsapenko, A. O. Skrypnyk, Yu. E. Logachev, and L. A. Gamayunova, *PAST, Series: «Plasma Physics»*, (6), 63 (2018). https://vant.kipt.kharkov.ua/ARTICLE/VANT_2018_6/article_2018_6_63.pdf
- [37] V. V. Bobkov, L. P. Tishchenko, Yu. I. Kovtunencko, A. B. Tsapenko, A. A. Skrypnyk, and L. A. Gamayunova, *J. Surf. Invest. X-ray, Synchrotron Neutron Tech.* **14**(5), 899 (2020). <http://link.springer.com/article/10.1134/S1027451020050031>
- [38] R. A. Causey, *J. Nucl. Mater.* **300**(2-3), 91 (2002). [https://doi.org/10.1016/S0022-3115\(01\)00732-2](https://doi.org/10.1016/S0022-3115(01)00732-2)
- [39] Y. Oya, M. Shimada, T. Tokunaga, H. Watanabe, N. Yoshida, Y. Hatano, R. Kasada, T. Nagasaka, A. Kimura, and K. Okuno, *J. Nucl. Mater.* **442**, S242 (2013). <http://doi.org/10.1016/j.jnucmat.2013.01.321>
- [40] Y. Niu, S. Suzuki, X. Zheng, Ch. Ding, J. Chen, W. Wang, Y. Oya, and K. Okuno, *J. Nucl. Mater.* **417**, 551 (2011). <http://doi.org/10.1016/j.jnucmat.2010.12.108>
- [41] Y. Zhang, W. Wang, H. Ren, W. Han, F. Liu, J. Yu, Sh. Peng, and K. Zhu, *Nucl. Instrum. and Methods B.* **307**, 357 (2013). <https://doi.org/10.1016/j.nimb.2013.04.026>
- [42] R. A. Anderl, D. F. Holland, and G. R. Longhurst, *J. Nucl. Mater.* **176-177**, 683 (1990). [https://doi.org/10.1016/0022-3115\(90\)90127-9](https://doi.org/10.1016/0022-3115(90)90127-9)
- [43] O. V. Ogorodnikova, K. Sugiyama, T. Schwarz-Selinger, T. Dürbeck, and M. Balden, *J. Nucl. Mater.* **419**, 194 (2011). <https://doi.org/10.1016/j.jnucmat.2011.07.023>
- [44] K. Katayama, K. Uehara, H. Date, S. Fukada, and H. Watanabe, *J. Nucl. Mater.* **463**, 1033 (2015). <https://doi.org/10.1016/j.jnucmat.2014.11.103>

- [45] L.P. Tishchenko, T.I. Peregon, Yu.I. Kovtunenکو, V.V. Bobkov, A.V. Onishchenko, and R.I. Starovoitov, *Bulletin of the Russian Academy of Sciences: Physics*, **70**(8), 1372 (2006). <https://www.elibrary.ru/item.asp?id=14370770>.
- [46] V.V. Bobkov, A.V. Onishchenko, O.V. Sobol, R.I. Starovoitov, Yu.I. Kovtunenکو, Yu.E. Logachev, and L.P. Tishchenko, *J. Surf. Invest. X-ray, Synchrotron Neutron Tech.* **4**(5), 852 (2010). <http://link.springer.com/article/10.1134/S1027451010050289>
- [47] V.V. Bobkov, L.P. Tishchenko, A.V. Onishchenko, E.N. Zubarev, R.I. Starovoitov, Yu.I. Kovtunenکو, Yu.E. Logachev, and L.A. Gamayunova, *J. Surf. Invest.: X-ray, Synchrotron and Neutron Tech.* **5**(4), 806 (2011). <http://link.springer.com/article/10.1134/S1027451011080052>
- [48] V.V. Bobkov, R.I. Starovoitov, L.P. Tishchenko, Yu.I. Kovtunenکو, and L.A. Gamayunova, *J. Surf. Invest.: X-ray, Synchrotron and Neutron Tech.* **8**(5), 853 (2014). <https://doi.org/10.1134/S1027451014030264>
- [49] V.V. Bobkov, L.P. Tishchenko, Yu.I. Kovtunenکو, R.I. Starovoitov, Yu.E. Logachev, A.B. Tsapenko, and L.A. Gamayunova, *Ukr. J. Phys.* **65**(1), 61 (2020). <https://doi.org/10.15407/ujpe65.1.61>
- [50] S. Krat, Yu. Gasparyan, Ya. Vasina, A. Davletiyarova, A. Pisarev, *Vacuum*. **149**, 23 (2018). <https://doi.org/10.1016/j.vacuum.2017.12.004>
- [51] Yu. Gasparyan, S. Krat, A. Davletiyarova, Ya. Vasina, and A. Pisarev, *Fusion Eng. Des.* **146**, 1043 (2019). <https://doi.org/10.1016/j.fusengdes.2019.01.154>
- [52] B.B. Cipiti, and G.L. Kulcinski, *J. Nucl. Mater.* **347**(3), 298 (2005). <https://doi.org/10.1016/j.jnucmat.2005.08.009>
- [53] V.V. Bobkov, L.P. Tishchenko, Yu.I. Kovtunenکو, A.O. Skrypnyk, and L.A. Gamayunova, *PAST, Series: «Plasma Physics»*, (6), 93 (2020). https://vant.kipt.kharkov.ua/ARTICLE/VANT_2020_6/article_2020_6_93.pdf
- [54] V.V. Bobkov, R.I. Starovoitov, L.P. Tishchenko, E.N. Zubarev, Yu.I. Kovtunenکو, Yu.E. Logachev, in: *Proceedings of the 20th International Conference on Ion-Surface Interactions*, (ISI-2011, Zvenigorod, 2011), Vol. **2**, pp. 61–64. (in Russian)
- [55] N.A. Azarenkov, V.V. Bobkov, L.P. Tishchenko, R.I. Starovoitov, Yu.I. Kovtunenکو, Yu.E. Logachev, and L.A. Gamayunova, *PAST, Series: «Plasma Physics»*, (6), 73 (2016). https://vant.kipt.kharkov.ua/ARTICLE/VANT_2016_6/article_2016_6_73.pdf
- [56] O.V. Ogorodnikova, N.S. Klimov, Yu.M. Gasparyan, Z.R. Harutyunyan, V.S. Efimov, D. Kovalenko, K. Gutarov, A.G. Poskakalov, M.M. Kharkov, and A.V. Kaziev, in: *Proceedings of the 25th International Conference on Ion-Surface Interactions*, (ISI-2021 Moscow, Russia, 2021), Vol. **1**, pp. 65–67.
- [57] S.A. Krat, E.A. Fefelova, A.S. Prishvitsyn, Yu.M. Gasparyan, and A.A. Pisarev, in: *Proceedings of the 25th International Conference on Ion-Surface Interactions*, (ISI-2021 Moscow, Russia, 2021), Vol. **1**, pp. 108–110. (in Russian)

ДОСЛІДЖЕННЯ ПРОЦЕСІВ ЗАХОПЛЮВАННЯ ТА ВИДІЛЕННЯ ІМПЛАНТОВАНИХ ІОНІВ ДЕЙТЕРІЮ ТА ГЕЛІЮ ДЛЯ ПЛІВОК ВОЛЬФРАМУ І ТАНТАЛУ

Микола Азаренков^b, Валентин Бобков^a, Людмила Тищенко^a, Юрій Ковтуненко^a, Анатолій Скрипник^a, Дмитро Шевченко^a, Любов Гамаюнова^a

^aХарківський національний університет імені В.Н. Каразіна, Харків, м. Свободи, 4, 61022, Україна

^bНаціональний науковий центр «Харківський фізико-технічний інститут», вул. Академічна, 1, Харків, 61108, Україна

Проведено аналіз основних наявних в літературі результатів досліджень накопичення та міграції іонно-імплантованих ізотопів водню та гелію у вольфрамівих і танталових покриттях, утворення радіаційних пошкоджень кристалічної решітки та їх взаємодії з імплантованими газами. Показано вплив гелію та дейтерію на різні властивості і морфологію поверхні покриттів. Опромінення зразків проводили як пучками прискорених іонів ізотопів водню або He⁺, так і у плазмі, яка містить перелічені іони, при різних дозах та енергіях падаючих іонів, різних температурах мішені при імплантації. Особливу увагу приділено результатам досліджень, отриманим при одночасному опроміненні W, як у масивному вигляді, так і в тонкоплівковому. Використовувалися методи електронної мікроскопії, ре-емісійної мас-спектрометрії, термодесорбційної спектрометрії, рентгенівської фотоелектронної спектроскопії, рентгенівської дифракції, аналізу ядерної реакції та резерфордівського розсіювання іонів.

Ключові слова: дейтерій; гелій; іонна імплантація; термодесорбція; дефекти; W і Ta плівки